JOURNAL OF GEOPHYSICAL RESEARCH, VOL. 101, NO. B2, PAGES 3269–3290, FEBRUARY 10, 1996

Glacial isostatic adjustment and Earth rotation: Refined constraints on the viscosity of the deepest mantle

W. R. Peltier and Xianhua Jiang

Department of Physics, University of Toronto, Toronto, Ontario, Canada

Abstract. We explore the extent to which two properties of Earth's present-day rotational state may be applied to constrain the viscosity of the lower regions of the lower mantle. The analysis builds upon recent advances in understanding the radial resolving power of the relative sea level data of postglacial rebound which have demonstrated anew that no significant increase of viscosity across the 660-km seismic discontinuity appears to be allowed by these data. Such observations do not constrain the viscosity of the mantle below about 1400 km depth, however, and here we estimate the average viscosity in this deepest region by invoking observations of the present-day rate and direction of polar wander and the present-day magnitude of the nontidal acceleration of the rate of planetary rotation. Since the rotational response to the glaciation cycle depends only upon the degree 2 spherical harmonic components of the induced deformation, this response is expected to provide the most specific sampling possible of deep mantle properties. Our analysis is based upon the use of glacial excitation functions calculated from complete gravitationally self-consistent solutions of the sea level equation for the most recent refinement of the history of ice sheet thickness variations across the last glacial-interglacial transition, namely, the ICE-4G model. This analysis shows that when Earth rotation observations are combined with relative sea level constraints, the viscosity of the deepest mantle is required to be ~1 order of magnitude higher than the viscosity of the upper part of the lower mantle. Such significant elevation of viscosity in the lowermost region of the lower mantle is also in accord with recent inferences based upon analysis of the nonhydrostatic geoid. The analyses presented herein therefore suffice to effect a reconciliation between the requirements of these distinct geophysical observations.

Introduction

Continuing observations of Earth's rotational state clearly demonstrate that the axis of rotation is fixed neither in space nor to the body of the planet itself, nor is the rate of rotation about the axis constant. Induced by a wide variety of complex internal and external processes, observed changes in rotational state span a broad spectrum of timescales ranging from hours to millions of years. Of the very wide range of rotational variations that do occur, we refer to as "polar wander" the secular drift of the axis of rotation with respect to a frame of reference fixed to the crust. From the turn of the century until 1982 the position of the north rotation pole of Earth relative to the crust fixed Conventional International Origin (CIO) was monitored by the International Latitude Service (ILS). Analyses of these data have clearly revealed that the mean position of the pole is currently drifting southward in a direction approximately aligned with the 76° west meridian of longitude at a rate near per 0.95° per m.y. [e.g., *Dickman*, 1977]. This observation, based upon the reduction of data from an array of northern hemisphere photo-zenith tubes, has more recently been corroborated using very long baseline interferometry observations from the radio telescopes contributing to the International Earth Rotation Service [*Carter et al.*, 1986].

Just as the earliest astronomical observations of polar wander have been largely replaced by modern space-based geodetic techniques, observations of the changing rate of rotation of Earth have been similarly influenced. In many ways the ongoing effort to understand long timescale changes in Earth's rate of axial rotation involves significantly greater complexity than does the problem posed by polar wander. Clearly this is because there exists a continuous exchange of angular momentum between Earth and the Moon that is mediated by tidal friction and which is responsible for a continuous increase in the length of day (decrease of the rate of rotation). That there existed some "anomaly" associated with this influence of tidal friction was first made clear [e.g., *Newton*, 1972; *Morrison*, 1973; *Muller and Stephenson*, 1975] on the basis of analyses of ancient eclipse data extending back to Babylonian times. These analyses demonstrated that there was a systematic error in the prediction of the times of occurrence of total eclipses of the Sun and Moon that were made on the basis of the assumption that tidal friction was constant, a systematic error such as to imply the action of an acceleration of rotation operating in opposition to the deceleration associated with tidal friction.

Paper number 95JB01963.
0148-0227/96/95JB-01963$05.00

These early estimates of the nontidal acceleration, expressed in terms of the ratio $\dot{\omega}_3/\Omega$ (in which Ω is the present angular velocity and $\dot{\omega}_3$ the angular acceleration about the rotation axis), ranged from 0.8×10^{-10} yr^{-1} to 3.0×10^{-10} yr^{-1}. In the very recent past it has proven possible using laser ranging data from the Lageos and Starlette satellites to measure the related quantity $\dot{J}_2$, the time derivative of the degree two axial component in the expansion of Earth's gravitational potential field, a parameter that is directly proportional to $\dot{\omega}_3/\Omega$. These modern space geodetic observations constrain $\dot{J}_2$ to the range between $(-2.5 \pm 0.3) \times 10^{-11}$/yr^{-1} and $(-3.5 \pm 0.3) \times 10^{-11}$ yr^{-1}, implying a value of $\dot{\omega}_3/\Omega$ that is very close to the lower limit of the range of values inferred from the ancient eclipse observations.

The history of the interpretation of these two Earth rotation observations is as interesting as are the observations themselves. First, concerning the true polar wander datum that we will explore in particular detail in the present paper, its possible connection to the glacial isostatic adjustment process was initially considered to be improbable. The reason for this has to do with an analysis by *Munk and MacDonald* [1960] which implied, on the basis of the assumption of a viscoelastic model Earth with uniform properties, that polar wander would cease immediately after the surface load on the system ceased to vary in time. In the case of the glacial isostatic adjustment process the surface load, of course, consists of the changing ice and water load associated with the growth and decay of continental ice sheets. Because the last deglaciation event of the current ice age ended approximately 6000 years ago, since which time the surface load has been stationary (except for a weak residual variation due to continuing redistribution of water among the ocean basins that accompanies the continuing relaxation of shape), it seemed on the basis of the *Munk and MacDonald* [1960] analysis that no significant current polar wander could be associated with this cause. *Peltier* [1982] and *Wu and Peltier* [1984], correcting an initial analysis of this problem by *Sabadini and Peltier* [1981], however, showed that more realistic viscoelastic models of the Earth behaved quite differently from the radially homogeneous model of *Munk and MacDonald* [1960]. This difference, in fact, as discussed below, is such that polar wander at the observed rate and in the observed direction is an entirely expected consequence of the last Pleistocene glaciation-deglaciation cycle if the viscosity of Earth's mantle is appropriately selected. Very little detailed analysis of the nature of the constraint on viscosity provided by the polar wander data has been presented, however, and it will be one of our purposes in the present paper to more fully analyze the nature of this constraint.

The interpretation of the nontidal acceleration of rotation/$\dot{J}_2$ observation has had a similar recent history of connection with the postglacial rebound process. *Peltier* [1982], interested by a lecture he had heard in Toronto by D. G. King-Hele on the prospects for measuring $\dot{J}_2$ using artificial satellite data, presented an initial analysis of the magnitude of the signal expected due to the glacial isostatic adjustment process and compared it to the inference based upon ancient eclipse data. The first reported measurement of $\dot{J}_2$ based upon laser ranging observations to the Lageos satellite was shortly thereafter published by *Yoder et al.* [1983], who attributed the signal to glacial isostasy, and *Peltier* [1983] presented a detailed analysis using realistic linear Maxwell models which further reinforced this interpretation. *Peltier* [1985] employed the $\dot{J}_2$ datum in demonstration of a new algorithm for inverting viscoelastic Love numbers into the time domain, an algorithm that now represents a most important step in the complete viscoelastic normal mode theory for glacial isostasy [*Peltier*, 1974, 1976, 1985]. To this point, all of the analyses of the rotational response to deglaciation had been based upon the use of extremely simple space-time models for the glaciation-deglaciation process, including that of *Peltier* [1988], who explored the magnitude of the impact on both polar wander and $\dot{J}_2$ of present-day glacial melting such as that due to small ice sheets and glaciers documented by *Meier* [1984]. In the case of $\dot{J}_2$ (in fact, for all $\dot{J}_\ell$ with $\ell \leq 10$) the validity of such approximate representations of the surface load was tested recently [*Mitrovica and Peltier*, 1993a,b] by employing the ICE-3G deglaciation model of *Tushingham and Peltier* [1991] coupled with a full gravitationally self-consistent solution of the sea level equation to fix the ocean component of the load. This analysis demonstrated that the previously employed approximation of the surface load had led to errors in the $\dot{J}_2$ calculations that were at most of order 10%, a very satisfying result indeed.

In the present paper, our main purpose is to more fully investigate, primarily through a sequence of analyses of the forward problems for the above discussed rotational data, the nature of the constraint on deep mantle viscosity that they provide. In this process our calculations will make use of the recently published ICE-4G deglaciation model [*Peltier*, 1994] which is the most detailed presently available and, in particular, considerably more accurate than the former ICE-3G model that it has been designed to replace. Our main goal will be to analyze the nature of the radial viscosity profile that is inferred from the rotational data when the constraints provided by relative sea level (rsl) information are simultaneously invoked. Recently published formal inversions of postglacial rsl data [*Mitrovica and Peltier* 1993a,b, 1995] have clearly demonstrated that such data demand that the radial profile of mantle viscosity to a depth of order 1200-1600 km be relatively uniform and near the observed value of 10^{21} Pa s originally inferred by *Haskell* [1935] on the basis of his analysis of the postglacial rebound of Fennoscandia. As we will show, both of the rotational observations agree that in the presence of this new formal constraint on the shallower structure of the mantle viscosity profile, the viscosity of the deeper mantle might be considerably higher, perhaps by approximately an order of magni tude.

Before proceeding to describe the new analyses that we have performed, it will be useful to first provide a brief review of the published quantitative estimates of the above described rotational observations. Estimates of present-day polar wander (the secular drift of the axis of Earth's rotation relative to a frame of reference fixed in crust) have been made by a number of authors based upon analyses of the photo-zenith tube data of the ILS. These ILS observational data [*Vincente and Yumi*, 1969] describe the position of the north rotation pole of Earth relative to the position of CIO and span the time period from 1900 until 1982. Figure 1 shows the ILS time series for the x and y components of the polar motion in a coordinate system oriented such that the x

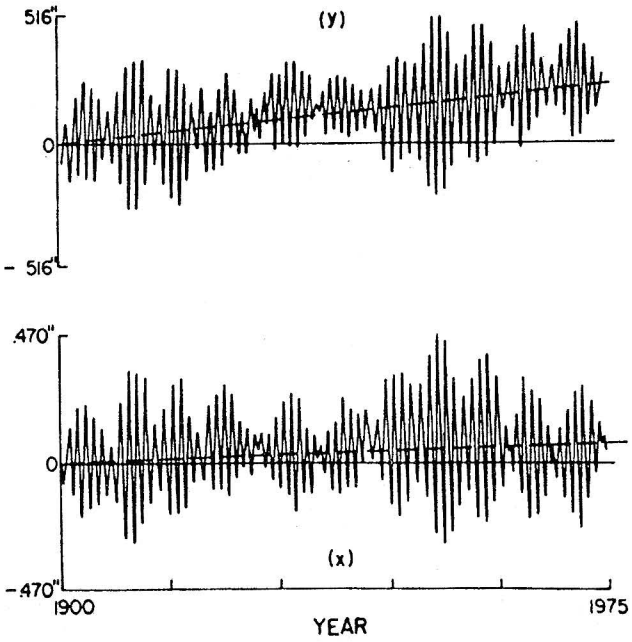

Figure 1. ILS time series for the x and y components of the polar motion since 1900. The dashed lines denote the secular drift which is occurring at the rate of approximately 0.95"/m.y.

axis passes through Greenwich and the y axis lies along the 90°W meridian. Inspection of these time series reveals them to be dominated by the 7-year beat period due to the interference between the 12-month annual forced oscillation and the 14-month Chandler free oscillation. The signal in these data that is of interest to us consists of the secular variation upon which this oscillatory component is superimposed. Figure 2a tabulates estimated values of polar wander speed based upon five different analyses which constrain this speed to lie between 0.8° and 1.1° m.y.$^{-1}$. Also tabulated on Figure 2a, however, is the independent estimate of polar wander speed based upon the interpretation of VLBI data by *Carter et al.* [1986] which lies just inside the upper bound of Dickman's estimate. In Figure 2b the direction of polar wander velocity estimated by *Dickman* [1977] is shown in north polar projection along with the orientation of the x and y axes of the conventional geodetic coordinate system. According to *Dickman* [1977], the direction of polar wander is along the 76°W meridian, a direction that lies somewhat to the east of the centroid of the Laurentian ice sheet which was centered upon Hudson Bay. This result was supported by the later analysis of *Vondrak* [1984], who found the direction of polar wander to be along the 78.2° meridian.

The secular variation of Earth's speed of axial rotation has also been determined on the basis of completely distinct observational methodologies. Using ancient records of solar and lunar eclipses ranging from 700 B.C. to 1600 A.D., *Stephenson and Morrison* [1995] recently reported an increase of the length of the mean solar day (l.o.d) of (1.70 ± 0.05) ms/yr, which implies a decrease of the angular speed of rotation of (-4.5 ± 0.1) x 10^{-22} rad/s^2 on the average over the last 2700 years. After subtracting from the total the contribution due to the tidal braking of Earth's spin, they obtained an average nontidal acceleration of Earth's rotation of (1.6 ± 0.4) x 10^{-22} rad/s^2 over the last 2700 years. This nontidal acceleration corresponds to a value for $\dot{J}_2$ of (-3.5 ± 0.8) x 10^{-11}.

The second experimental technique that has been used to infer the magnitude of the nontidal component of the acceleration of rotation has involved measurement of the acceleration of the node of the orbit of an artificial satellite, a characteristic of the orbit which is directly associated with the time dependence of the degree 2 axial component of Earth's gravitational potential field J_2 (more accurately, this observation is influenced by all of the axial components of even degree, but most strongly by degree 2). Using satellite laser ranging (SLR) measurements to the Starlette and Lageos satellites, the time rate of change of J_2 has been determined in several published analyses [e.g., *Yoder et al.*, 1983; *Rubincam*, 1984; *Cheng et al.*, 1989; *Gegout and Caznave*, 1991]. The values of $\dot{J}_2$ determined by this methodology range from -2.5 x 10^{-11} yr^{-1} to -3.5 x 10^{-11} yr^{-1}, and these are consistent with the results obtained from the above described analyses of ancient eclipse data. Figure 3 tabulates five published values for $\dot{J}_2$ and their associated error bars as determined by the application of these two methodologies. It is important to note that the value most recently inferred on the basis of the eclipse observations by *Stephenson and Morrison* [1995] is essentially identical to the inference by *Yoder et al.* [1983] on the basis of Lageos laser ranging data, although the error bars are larger.

The outline of the remainder of this paper is as follows. We provide a complete gravitationally self-consistent theory of the rotational response to the glaciation-deglaciation process, focusing especially upon the manner in which the full influence of variable ocean basin bathymetry may be integrated into the analysis. A considerable extension of the previous analyses of *Peltier* [1982] and *Wu and Peltier* [1984] of the polar wander response will also be recorded. This extension to previously published theory involves accounting for the full influence of gravitational triaxiality on the polar wander effect. We then detail the results obtained by application of this more fully elaborated theory to understanding the nature of the constraint on deep Earth viscosity structure that the observed rotational data provide.

A Complete Theory of the Rotational Response to the Glaciation-Deglaciation Cycle

The main improvement to the theory of glaciation induced rotational effects that we will elaborate here concerns the accuracy with which the ice and water components of the surface load are described. Given the space and time dependent variations of ice thickness, it is by now well known that the "sea level equation" [e.g., *Peltier et al.*, 1978] may be solved to accurately predict the variation of ocean bathymetry that must accompany the variations of ice thickness. This equation enables a gravitationally self-consistent accounting of the manner in which water is continuously redistributed over the surface of the deglaciating earth in order that the surface of the ocean continue to lie on a gravitational equipotential. In all past analyses of the polar wander induced by the glacial cycle both the oceanic and cryospheric components of the surface load have been approximated; in the case of the ice load the individual continental ice sheets have been approximated by simple

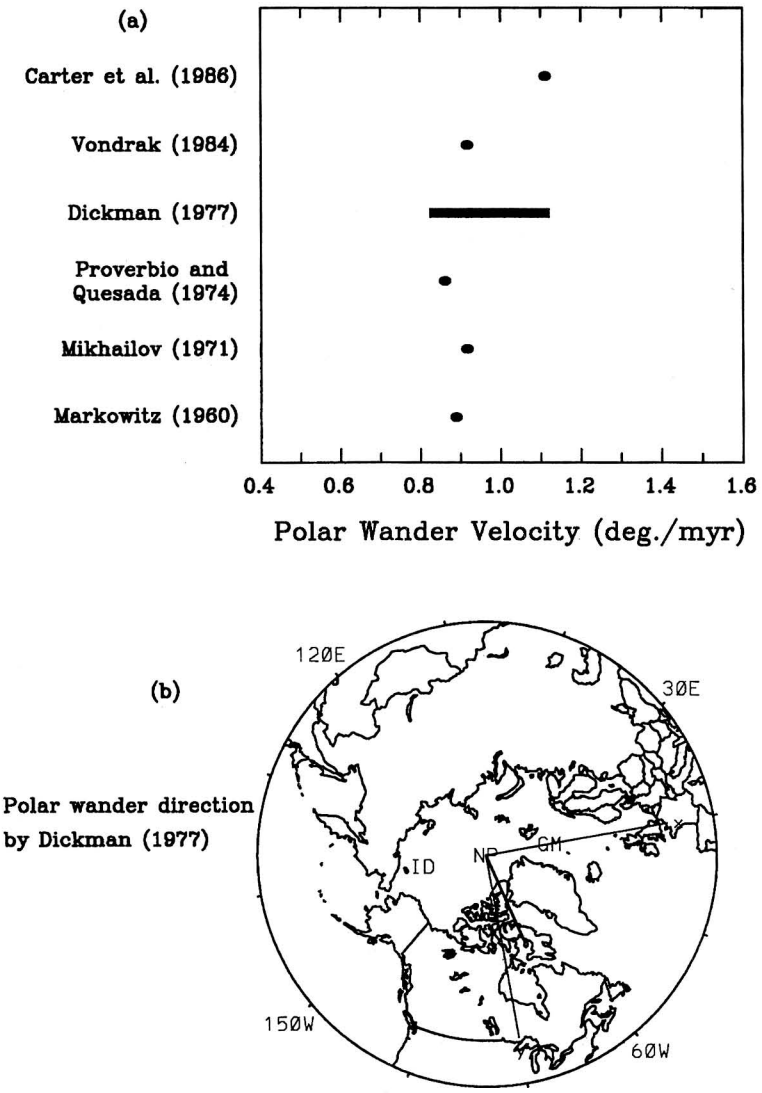

Figure 2. Various inferences of the polar wander speed and direction. (a) Six observed values of polar wander speed. The value presented by *Carter et al.* [1986] is estimated on the basis of VLBI observations, while the remaining five values are based upon the ILS data shown in Figure 1. (b) The direction of present-day polar wander along the 76°W meridian obtained by *Dickman* [1977], a direction which is skewed somewhat to the east of the centroid of the Laurentian ice sheet.

circular disks with temporal variability represented by 100 kyr periodic saw-tooth functions that roughly mimic the history of the ice volume variations inferred on the basis of oxygen isotope data from deep-sea sedimentary cores [e.g., *Imbrie et al.*, 1984; *Shackleton et al.*, 1990]. Similarly, the ocean component of the load has been approximated as eustatic; that is, the variations of ocean bathymetry forced by ice sheet accretion and disintegration have been treated as being independent of spatial position within the ocean basins. Although these assumptions have recently been relaxed in the analysis of the $\dot{J}_2$ datum [*Mitrovica and Peltier*, 1993a], there has been no previous attempt to account for polar wander observations using a complete gravitationally self-consistent theory.

Very recently, a number of significant advances have also been achieved in the development of the gravitationally self-consistent theory itself and in the improvement of our knowledge of the glaciation-deglaciation process. In the former area we now have available [*Peltier*, 1994] a topographically self-consistent version of the theory which accurately includes the influence of the variation through time of the ocean function caused by inundation of the continents due to rising sea levels and the elevation of continental regions above the level of the sea due to glacial rebound. This improved theory has also been combined with new data to further refine our knowledge of the spatial-temporal characteristics of the last deglaciation event, thus leading to the development of the ICE-4G model [*Peltier*, 1994], a model that is a very significant improvement on the previous ICE-3G version [*Tushingham and Peltier*, 1991]. A further improvement in the basic numerical methods that are employed to solve the sea level equation has also been achieved with the successful implementation of a spherical harmonics based methodology [*Mitrovica and Peltier*, 1991] that corrects a number of deficiences in the finite element techniques that were previously employed to invert this integral equation [e.g.. *Peltier et al.*, 1978; *Tushingham and Peltier*, 1991]. In the new analysis of Earth's rotational

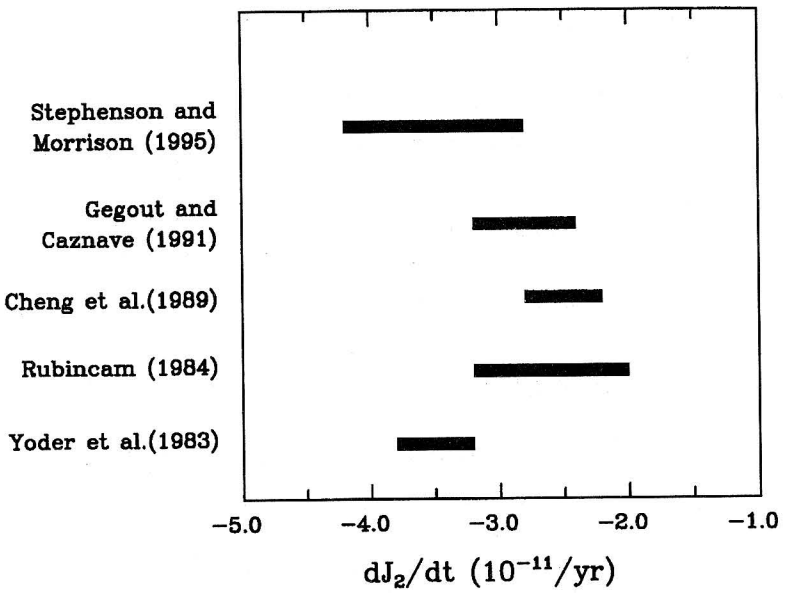

Figure 3. Various inferences of present-day $\dot{J}_2$. The value of *Stephenson and Morrison* [1995] is based upon the analysis of ancient eclipse data, while the remainder are based upon observations of satellite orbits.

response to the glacial cycle that constitutes the focus of this paper, all of these recent advances will be applied to obtain the most accurate analysis of rotational effects that is currently feasible.

Gravitationally Self-Consistent Solutions of the Sea Level Equation for ICE-4G

The sea level equation, whose solution delivers a prediction of the variations of the level of the sea $S(\theta, \lambda, t)$ relative to the isostatically adjusting surface of the solid Earth, may be written

$$S(\theta,\lambda,t) = C(\theta,\lambda,t)\,[G(\theta,\lambda,t) - R(\theta,\lambda,t)]\,, \quad (1a)$$

or, representing G and R explcitly, as

$$S(\theta,\lambda,t) = C(\theta,\lambda,t)\left[\int_{-\infty}^{t}\int\!\!\int_{\Omega} L(\theta',\lambda',t') \cdot \left(\frac{\phi(\gamma,t-t')}{g} - \Gamma(\gamma,t-t')\right) d\Omega'\,dt' + \frac{\Delta\Phi}{g}\right] \quad (1b)$$

in which $G(\theta, \lambda, t)$ and $R(\theta, \lambda, t)$ are the temporally evolving variations, both measured in meters, of the geoid and Earth's solid surface, respectively. The function $C(\theta, \lambda, t)$ is the ocean function, by definition equal to unity over the oceans and equal to zero over the continents. In (1b) the function $L(\theta, \lambda, t)$ is the surface load, consisting of distinct ice and ocean components, and this may be usefully expanded in a form that recognizes explicitly this composite property, as

$$L(\theta,\lambda,t) = \rho_I I(\theta,\lambda,t) + \rho_w S(\theta,\lambda,t)\,, \quad (1c)$$

in which ρ_I and ρ_W are the densities of ice and water, and I and S are the thicknesses of these distinct components of the surface load. Since S appears both under the triple integral on the right side of (1b) and on the left-hand side, (1c) is an integral equation. The kernel in this integral equation consists of Green functions for the surface mass load boundary value problem, those for the gravitational potential perturbation (ϕ) and the radial displacement (Γ), respectively, the construction of which has been described in detail elsewhere [*Peltier* 1974, 1976, 1985]; (see the review by *Peltier* [1989] for a recent summary). The remaining function in (1b), $\Delta\Phi(t)$, is defined as

$$\frac{\Delta\Phi(t)}{g} = -\frac{M_I(t)}{\rho_W A_0} - \frac{1}{A_0}\left\langle \int_{-\infty}^{t}\int\!\!\int_{\Omega} L(\theta',\lambda',t') \cdot \left[\frac{\phi(\gamma,t-t')}{g} - \Gamma(\gamma,t-t')\right] d\Omega'\,dt' \right\rangle . \quad (1d)$$

This time dependent number is fixed by the requirement that the integral of the product $\rho_W S(\theta, \lambda, t)$ over the ocean basins, indicated by the angle brackets in (1d), be equal to $M_I(t)$ which is the mass lost by the ice sheets in melting by time t. This adjustment then ensures that the separation between G and R that is driven by the deglaciation process is constrained by the conservation of mass in the surface load. The quantity A_0 that appears in (1d) is just the area of the oceans, and this is not necessarily constant since the ocean function C will, in general, be time dependent as water inundates low lying regions of the continents during deglaciation and as water-covered regions emerge from the sea as a consequence of postglacial rebound of the crust in regions that are initially ice covered.

Given a model of the deglaciation process represented by $I(\theta, \lambda, t)$, this may be input to (1b)-(1c) and the integral equation inverted continuously in time to obtain the globally defined field $S(\theta, \lambda, t)$, which is the predicted time dependent separation between the geoid and the surface of the solid Earth. Where there is ocean, $S(\theta, \lambda, t)$ is the predicted variation of the level of the sea with respect to the deforming

surface of the solid Earth. This gravitationally self-consistent solution $S(\theta, \lambda, t)$ may be made topographically self-consistent [*Peltier*, 1994] simply by noting that being a result of the application of first-order perturbation theory relative to an arbitrary initial state, we are free to adjust $S(\theta, \lambda, t)$ by adding to it an arbitrary time independent initial field. If we choose this field $T'(\theta, \lambda)$ such that

$$S(\theta, \lambda, t_p) + T'(\theta, \lambda) = T_p(\theta, \lambda), \qquad (2)$$

where T_p is the present topography of Earth with respect to sea level and t_p is the present time, then the topography of the rocky part of the planet relative to sea level at all times t will just be

$$T(\theta, \lambda, t) = S(\theta, \lambda, t) + [T_p(\theta, \lambda) - S(\theta, \lambda, t_p)] \qquad (3)$$

in which the total paleotopography, including the contribution due to the thickness of the ice, will clearly be

$$PT(\theta, \lambda, t) = T(\theta, \lambda, t) + I(\theta, \lambda, t) \ . \qquad (4)$$

As discussed by *Peltier* [1994], equation (4) provides us with a means of computing the time dependence of the ocean function $C(\theta, \lambda, t)$ that appears in (1a) and (1b) since where PT is negative, there is ocean, whereas where PT is positive, there is (perhaps ice-covered) continent. Since the temporal variations in $C(\theta, \lambda, t)$ are modest, we may determine their history in an iterative fashion. We first fix $C(\theta, \lambda, t) = C(\theta, \lambda, t_p)$ and determine a first guess $C^1(\theta, \lambda, t)$ from (4). We then solve (1) again using $C^1(\theta, \lambda, t)$ to determine a next guess $C^2(\theta, \lambda, t)$ from (4) and continue until acceptable convergence is achieved. This typically requires no more than two to three iterations when (1) is inverted on a basis of spherical harmonics truncated at degree and order 512.

For the purpose of the rotational analysis to be presented in what follows we have solved (1) using as input the new ICE-4G model of the deglaciation process derived by *Peltier* [1994] for the time from glacial maximum to the present. For the extensive period of the Pleistocene prior to glacial maximum we have employed the methodology described by *Peltier and Jiang* [1994] that is based upon the so-called SPECMAP $\delta^{18}O$ record of *Imbrie et al.* [1984]. Acceptably accurate assessments of the impact of initial glacial isostatic disequilibrium are thereby calculated by assuming that prior to the last glacial maximum (LGM) the ice sheets maintained their LGM spatial form and simply varied in thickness in a manner linearly related to the instantaneous $\delta^{18}O$ anomaly from LGM. We therefore integrate (1) over a time period of 780,000 years in order to develop predictions of the variations of surface load with time that may be employed to calculate the rotational excitation functions needed to determine the rotational response to the ice age cycle.

As an example of a solution of (1) obtained using the ICE-4G deglaciation history with the prehistory of loading and unloading constrained by the SPECMAP $\delta^{18}O$ record, we first show in in Plate 1 a sequence of northern hemisphere maps of the ICE-4G model of deglaciation from LGM to the present that illustrates the nature of the input to (1) for the last 21,000 years. In Plate 2 we present a sequence of maps of the rate of relative sea level rise corresponding to the times 20,000 years before present (kyr B.P.), 15 kyr B.P., 5 kyr B.P., and present day. For the purpose of this representative analysis the relative sea level history $S(\theta, \lambda, t)$ was obtained on the basis of an assumed model for mantle viscosity in which the lithosphere is taken to be 120 km thick, the viscosity of the mantle is taken to be equal to 10^{21} Pa s from the base of the lithosphere to a depth of 1400 km and the lowermost part of the lower mantle beneath this depth is taken to have a viscosity of 2×10^{22} Pa s. As we will discuss, a model of this general type has been suggested by a variety of recent analyses. For this particular calculation the time dependence of the ocean function was not included. Inspection of Plate 2 demonstrates the process of continuous redistribution of water among the ocean basins subsequent to the onset of deglaciation that is required to ensure that the surface of the ocean remain a gravitational equipotential. It is just this continuing additional forcing that is not captured by the previous analyses of the rotational response to deglaciation in which it has been assumed that the ocean component of the surface load could be treated as eustatic. In what follows we shall carefully incorporate the impact of this "deviation from eustatic" effect upon the rotational response to the glacial cycle for both polar wander and the nontidal acceleration.

Theory of Ice Age Induced Rotational Effects

All variations of the rotational state of the Earth system caused by glaciation and deglaciation are ultimately connected to variations in the elements of the inertia tensor (J_{ij}) forced by the changing surface load. In the presence of such load-induced changes of the inertia tensor, conservation of angular momentum then requires an adjustment of angular velocity (with components ω_i, say). These two variables are of course linked by the classical Euler equation which expresses this principle of conservation. In an Earth-fixed frame of reference rotating at angular velocity ω, these equations take the form [e.g., *Goldstein*, 1980]

$$\frac{d}{dt}(J_{ij}\,\omega_j) + \varepsilon_{ijk}\,\omega_j J_{k\ell}\,\omega_\ell = 0 \ , \qquad (5)$$

in which J_{ij} is the time dependent inertia tensor, ω_j is the jth component of the angular velocity vector, and ε_{ijk} is the Levi-Cevita (alternating) tensor. If we suppose that ω never departs significantly from its initial value (Ω, say), then (5) may be linearized by introduction of the following perturbation expansions:

$$\omega_i = \Omega(\delta_{i3} + m_i) \qquad (6a)$$

$$J_{ij} = I_{ij}, \quad i \neq j \qquad (6b)$$

$$J_{11} = A + I_{11} \qquad (6c)$$

$$J_{22} = B + I_{22} \qquad (6d)$$

$$J_{33} = C + I_{33} \ . \qquad (6e)$$

Here A, B, and C are the three principal moments of inertia, Ω is the mean angular velocity of Earth, the m_i are the dimensionless perturbations of the components of the angular velocity vector ω, and I_{ij} are the perturbations of inertia.

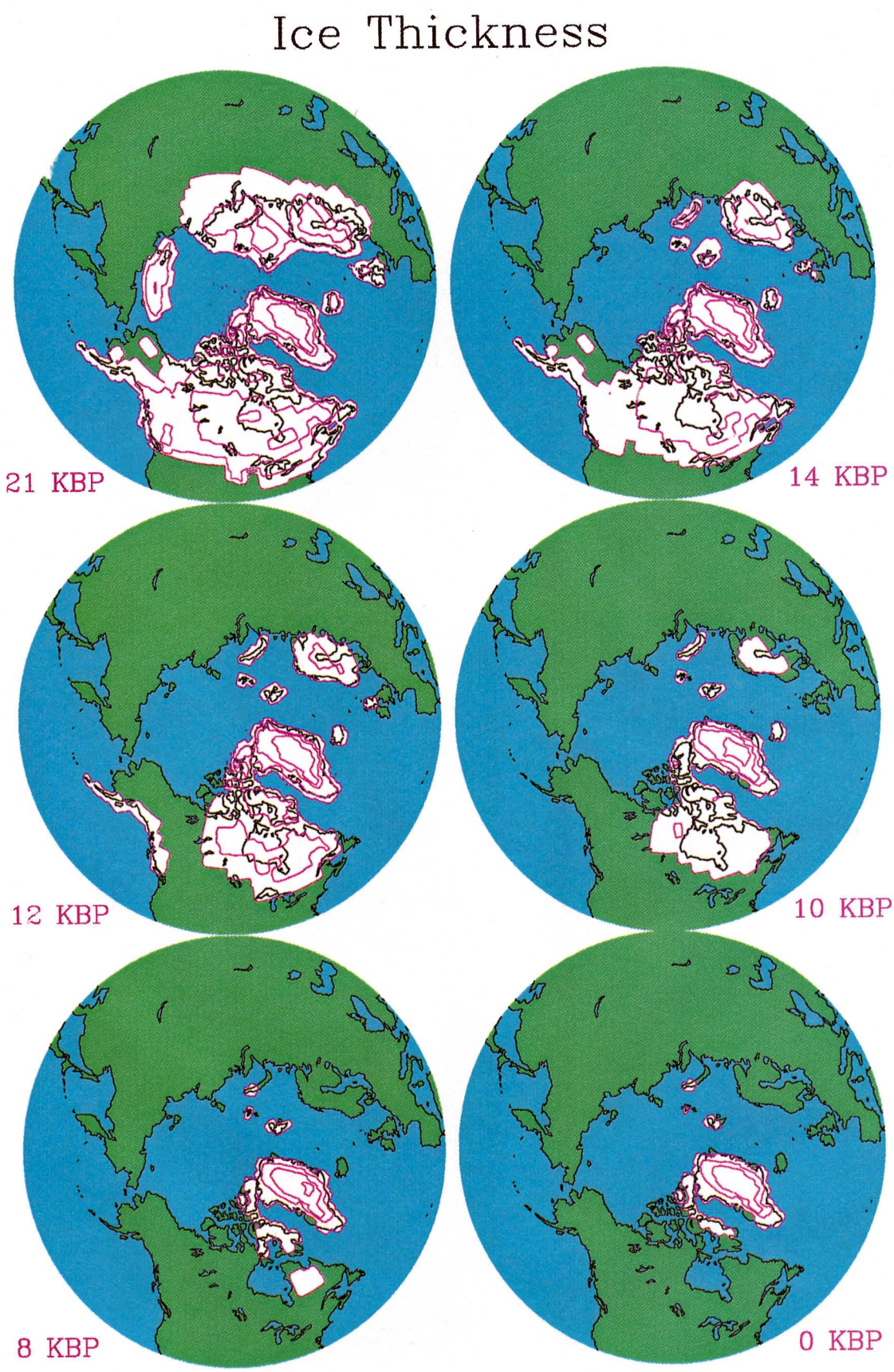

Plate 1. Time variation of ice sheet thickness based upon the ICE-4G deglaciation model of [*Peltier*, 1994] for a sequence of times beginning at LGM at 21 kyr ago and ending at the present. The contour interval is 1 km.

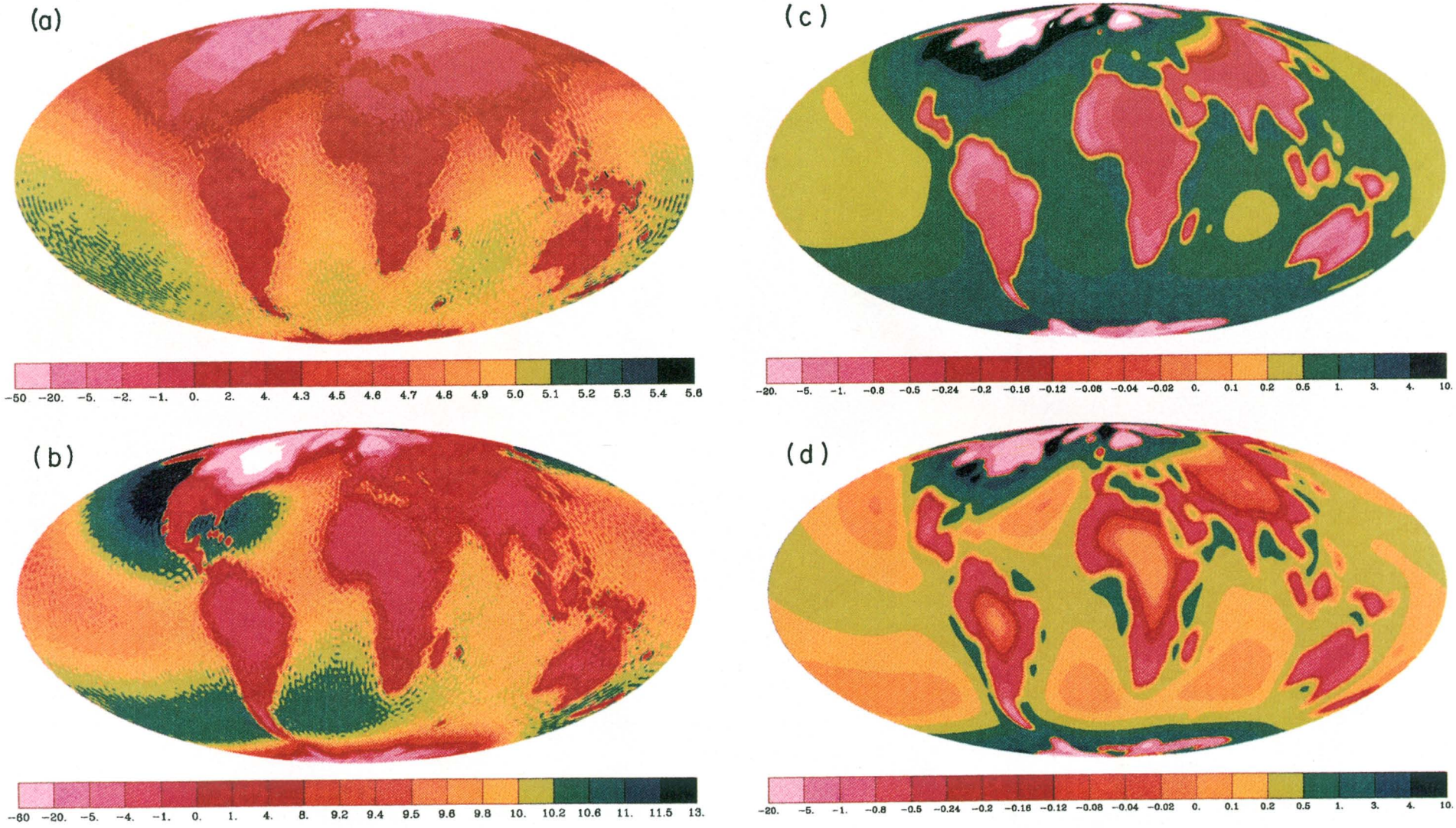

Plate 2. Rate of relative sea level rise in millimeters per year at four times: (a) 20,000 years ago when the last deglaciation event had just begun, (b) 10,000 years ago, (c) 5000 years ago by which time the last deglaciation event had ended and (d) present day.

Substitution of (6) into (5) followed by linearization leads to three equations for the m_j, namely,

$$\dot{m}_1 + \frac{C-B}{A}\Omega m_2 = \tilde{\Psi}_1 \tag{7a}$$

$$\dot{m}_2 - \frac{C-A}{B}\Omega m_1 = \tilde{\Psi}_2 \tag{7b}$$

$$\dot{m}_3 = \tilde{\Psi}_3 \tag{7c}$$

in which the so-called excitation functions are given by

$$\tilde{\Psi}_1 = \frac{\Omega}{A} I_{23} - \frac{\dot{I}_{13}}{A} \tag{8a}$$

$$\tilde{\Psi}_2 = -\frac{\Omega}{B} I_{13} - \frac{\dot{I}_{23}}{B} \tag{8b}$$

Including the contribution to the excitation functions from the rotational deformation itself [*Munk and MacDonald*, 1960], in the domain of Laplace transform variable s [*Wu and Peltier*, 1984], we can rewrite the two equations for polar wander (7a) and (7b) as

$$\tilde{\Psi}_3 = -\frac{I_{33}}{C} . \tag{8c}$$

$$s m_1 + (\sigma_2 - \sigma_1 k_2^T / k_f) m_2 = \tilde{\Psi}_1(s) \tag{9a}$$

$$-(\sigma_3 - \sigma_1 k_2^T / k_f) m_1 + s m_2 = \tilde{\Psi}_2(s) \tag{9b}$$

in which $\sigma_1 = \Omega(C - A)/A$, $\sigma_2 = \Omega(C - B)/A$ and $\sigma_3 = \Omega(C - A)/B$, k_2^T is the tidal Love number of degree 2, and k_f is the fluid Love number of degree 2 defined by $k_f = 3(C - A)G/(a^5\Omega^2)$. The Laplace transforms of the excitation functions are simply

$$\tilde{\Psi}_1(s) = \frac{\Omega}{A} I_{23}(s) - \frac{s}{A} I_{13}(s) \tag{10a}$$

$$\tilde{\Psi}_2(s) = -\frac{\Omega}{B} I_{13}(s) - \frac{s}{B} I_{23}(s) . \tag{10b}$$

It has been demonstrated [*Peltier*, 1982; *Wu and Peltier*, 1984] that the Laplace transforms of the I_{ij} themselves can be expressed in the form

$$I_{ij}(s) = [1 + k_2^L(s)] I_{ij}^R(s) \tag{11}$$

in which k_2^L is the surface load Love number of degree 2. Through the use of (10) and (11) the solutions to (9) for $m_1(s)$ and $m_2(s)$ may be seen to take the form

$$m_1(s) = H_1(s) I_{13}^R(s) + H'(s) I_{23}^R(s) \tag{12a}$$

$$m_2(s) = H_2(s) I_{23}^R(s) - H''(s) I_{13}^R(s) \tag{12b}$$

in which

$$H_1(s) = \frac{1 + k_2^L(s)}{\gamma(s)} \left[\frac{\Omega}{B}(\sigma_2 - \sigma_1 k_2^T(s)/k_f) - \frac{s^2}{A} \right] \tag{13a}$$

$$H'(s) = \frac{s(1 + k_2^L(s))}{\gamma(s)} \left[\frac{\Omega}{A} + \frac{1}{B}(\sigma_2 - \sigma_1 k_2^T(s)/k_f) \right] \tag{13b}$$

$$H_2(s) = \frac{1 + k_2^L(s)}{\gamma(s)} \left[\frac{\Omega}{A}(\sigma_3 - \sigma_1 k_2^T(s)/k_f) - \frac{s^2}{B} \right] \tag{13c}$$

$$H''(s) = \frac{s(1 + k_2^L(s))}{\gamma(s)} \left[\frac{\Omega}{B} + \frac{1}{A}(\sigma_3 - \sigma_1 k_2^T(s)/k_f) \right] \tag{13d}$$

$$\gamma(s) = s^2 + (\sigma_2 - \sigma_1 k_2^T(s)/k_f)(\sigma_3 - \sigma_1 k_2^T(s)/k_f) . \tag{13e}$$

Inspection of (13) clearly shows that if we let $A = B$ and neglect quantities of order s/σ_1, the approximation employed by *Wu and Peltier* [1984], then $H'(s)$ and $H''(s)$ are negligible and (12) reduce to equation (70) of *Wu and Peltier* [1984] which was obtained for a biaxial Earth model for which m_1 is only dependent upon I_{13}^R and m_2 upon I_{23}^R. As demonstrated by (15), for a more realistic triaxial Earth model both components of the polar wander vector are dependent upon the perturbations of both of the equatorial moments of inertia. In the time domain the two components of the polar wander vector are therefore determined to be:

$$m_1(t) = H_1(t) * I_{13}^R(t) + H'(t) * I_{23}^R(t) \tag{14a}$$

$$m_2(t) = H_2(t) * I_{23}^R(t) - H''(t) * I_{13}^R(t) \tag{14b}$$

in which the asterisk denotes the operation of convolution in the time domain and the time series $I_{13}^R(t)$ and $I_{23}^R(t)$ are to be directly computed from the history of ice and ocean loading. To perform the time convolutions in (14), we need the inverse Laplace transforms of $H_1(s)$, $H_2(s)$, $H'(s)$, and $H''(s)$.

In the present, more detailed, analysis we shall only neglect quantities of order of s^2/σ_j^2 in (13) since s/σ_j is of the same order as the equatorial flattening of the triaxial Earth upon which we are now focusing. This approximation reduces $H_1(s)$ to the form

$$H_1(s) = \frac{\Omega}{B} \frac{1 + k_2^L(s)}{\sigma_3 - \sigma_1 k_2^T(s)/k_f} . \tag{15}$$

Using the following expressions for the tidal Love number $k_2^T(s)$ and the load Love number $k_2^L(s)$ in the Laplace transform domain

$$k_2^T(s) = k_2^T(0) - s \sum_{j=1}^{N} \frac{t_j / s_j}{s + s_j} \tag{16a}$$

$$k_2^L(s) = -1 + l_s - s\sum_j^N \frac{r_j/s_j}{s+s_j} \tag{16b}$$

we can clearly rewrite $H_1(s)$ in the form

$$H_1(s) = \frac{\Omega}{B}\left[l_s - s\sum_{j=1}^N \frac{r_j}{s_j(s+s_j)}\right]\prod_{j=1}^N (s+s_j)/Q_N(s) \tag{17}$$

with

$$Q_N(s) = (\sigma_3 - \sigma_1 k_2^T(0)/k_f)\prod_{j=1}^N (s+s_j)$$

$$+ s\sigma_1/k_f \sum_{j=1}^N \frac{t_j}{s_j}\prod_{i\neq j}^N (s+s_i) = \prod_{j=1}^N (s+\lambda_j) \tag{18}$$

in which $\lambda_1, \ldots, \lambda_N$ are the N roots of $Q_N(s)$. To perform the inverse Laplace transform, we further rewrite $H_1(s)$ as

$$H_1(s) = \frac{\Omega}{B} l_s\left[1 - \frac{q(s)}{Q_N(s)}\right] - \frac{\Omega}{B}\sum_{j=1}^N \frac{r_j}{s_j}\left[1 - \frac{R_j(s)}{Q_N(s)}\right] \tag{19}$$

with

$$q(s) = \prod_{j=1}^N (s+\lambda_j) - \prod_{j=1}^N (s+s_j) \tag{20a}$$

$$R_j(s) = \prod_{j=1}^N (s+\lambda_j) - s\prod_{i\neq j}^N (s+s_i)\ . \tag{20b}$$

Given these factorizations, we may simply invert $H_1(s)$ into the time domain to obtain

$$H_1(t) = \frac{\Omega}{B}\left[l_s - \sum_{j=1}^N \frac{r_j}{s_j}\right]\delta(t) + \frac{\Omega}{B}\left[\sum_{i=1}^N E_i e^{-\lambda_i t}\right] \tag{21}$$

in which the E_i are defined as

$$E_i = \left[l_s q(-\lambda_i) + \sum_{j=1}^N \frac{r_j}{s_j} R_j(-\lambda_i)\right] \Big/ \prod_{k\neq i}^N (\lambda_k - \lambda_i)\ . \tag{22}$$

To find the inverse Laplace transform of $H'(s)$, we may begin by expressing it in the form

$$H'(s) = \frac{\Omega}{B}\frac{q_{2N+1}(s)}{Q_{2N+2}(s)}\ , \tag{23}$$

in which $q_{2N+1}(s)$ and $Q_{2N+2}(s)$ are polynomials of degree $2N+1$ and $2N+2$, respectively, given by the explicit expressions

$$q_{2N+1}(s) = \left[s\, l_s \prod_{j=1}^N (s+s_j) - s^2\sum_{j=1}^N \frac{r_j}{s_j}\prod_{i\neq j}^N (s+s_j)\right]$$

$$\cdot\left[\left(\frac{B}{A} + \frac{1}{\Omega}(\sigma_2 - \sigma_1 k_2^T(0)/k_f)\prod_{j=1}^N (s+s_j)\right.\right.$$

$$\left.\left. + \sigma_1/k_f\, s\sum_{j=1}^N \frac{t_j}{s_j}\prod_{i\neq j}^N (s+s_i)\right)\right] \tag{24a}$$

$$Q_{2N+2}(s) = \prod_{j=1}^N (s+s_j)\prod_{k=1}^N (s+s_k)\,[s^2 + \sigma_2\sigma_3$$

$$- \sigma_1(\sigma_2+\sigma_3)k_2^T(0)/k_f + \sigma_1^2 k_2^T(0)/k_f]$$

$$+ [\sigma_1(\sigma_2+\sigma_3)/k_f - \sigma_1^2 k_2^T(0)/k_f^2]\, s\sum_{j=1}^N \frac{t_j}{s_j}$$

$$\cdot\prod_{k=1}^N (s+s_k) + s^2\sum_{j=1}^N \frac{t_j}{s_j}\prod_{i\neq j}^N (s+s_i)\sum_{\ell=1}^N \frac{t_\ell}{s_\ell}\prod_{k\neq \ell}^N (s+s_k)\ . \tag{24b}$$

The inverse Laplace transform of $H'(s)$ is then

$$H'(t) = \frac{\Omega}{B}\sum_{i=1}^{2N+2} E_i' e^{-\lambda_i' t} \tag{25}$$

where λ_i' are the $2N+2$ roots of $Q_{2N+2}(s)$ and E_i' are given by

$$E_i' = q_{2N+1}(-\lambda_i') \Big/ \prod_{k\neq i}^{2N+2} (\lambda_k' - \lambda_i')\ . \tag{26}$$

Substitution of (21) and (25) into (14) leads to the final form of the solution for $m_1(t)$ in the time domain. Simply noticing that $H_2(s)$ and $H''(s)$ can be obtained by substituting σ_3 for σ_2 and exchanging B for A in the expressions for $H_1(s)$ and $H'(s)$, the inverse Laplace transform of $m_2(s)$ is the same as that for $m_1(s)$ discussed above. The two components of the polar wander vector then take the form

$$m_1(t) = \frac{\Omega}{B}\left[\ell_s - \sum_{j=1}^N \frac{r_j}{s_j}\right] I_{13}^R(t)$$

$$+ \frac{\Omega}{B}\left[\sum_{i=1}^N E_i e^{-\lambda_i t} * I_{13}^R(t) + \sum_{i=1}^{2N+2} E_i' e^{-\lambda_i' t} * I_{23}^R(t)\right] \tag{27a}$$

$$m_2(t) = \frac{\Omega}{A}\left[\ell_s - \sum_{j=1}^N \frac{r_j}{s_j}\right] I_{23}^R(t)$$

$$+ \frac{\Omega}{A}\left[\sum_{i=1}^N F_i e^{-\beta_i t} * I_{23}^R(t) - \sum_{i=1}^{2N+2} F_i' e^{-\beta_i' t} * I_{13}^R(t)\right] \tag{27b}$$

in which parameters β_i, F_i, β_i', and F_i' are computed using the same expressions for λ_i, E_i, λ_i', and E_i' where we substitute σ_3 for σ_2 and exchange A for B. These are the general expressions for the two components of the polar wander vector

induced by the surface load associated with the glaciation-deglaciation process for a triaxial viscoelastic model of Earth. To obtain the components of the polar wander velocity vector, we simply differentiate (27) with respect to time to obtain

$$\dot{m}_1(t) = \frac{\Omega}{B}\sum_{i=1}^{N} E_i I_{13}^R(t) + \frac{\Omega}{B}\left[\ell_s - \sum_{j=1}^{N}\frac{r_j}{s_j}\right]\dot{I}_{13}^R(t) + \frac{\Omega}{B}\sum_{i=1}^{2N+2} E_i' I_{23}^R(t) + M_1(t) * I_{13}^R(t) + M'(t) * I_{23}^R(t) \quad (28a)$$

$$\dot{m}_2(t) = \frac{\Omega}{A}\sum_{i=1}^{N} F_i I_{23}^R(t) + \frac{\Omega}{A}\left[\ell_s - \sum_{j=1}^{N}\frac{r_j}{s_j}\right]\dot{I}_{23}^R(t) + \frac{\Omega}{A}\sum_{i=1}^{2N+2} F_i' I_{23}^R(t) + M_2(t) * I_{23}^R(t) + M''(t) * I_{13}^R(t) \quad (28b)$$

Examination of (28) indicates that the polar wander response of Earth to the perturbations of inertia caused by the glaciation-deglaciation process may be considered to consist of an instantaneous elastic response and a viscous response. The elastic part would clearly make no contribution to predicted present-day polar wander velocity if it were assumed that at present no variation of the surface load was occurring since the present-day perturbations of inertia would then be zero. The viscous responses are completely determined by the four time dependent functions $M_1(t)$, $M'(t)$, $M_2(t)$, and $M''t)$ defined as

$$M_1(t) = -\frac{\Omega}{B}\sum_{i=1}^{N}\lambda_i E_i e^{-\lambda_i t} \quad (29a)$$

$$M'(t) = -\frac{\Omega}{B}\sum_{i=1}^{2N+1}\lambda_i' E_i' e^{-\lambda_i' t} \quad (29b)$$

$$M_2(t) = -\frac{\Omega}{A}\sum_{i=1}^{N}\beta_i F_i e^{-\beta_i t} \quad (29c)$$

$$M''(t) = -\frac{\Omega}{A}\sum_{i=1}^{2N+1}\beta_i' F_i' e^{-\beta_i' t}\ . \quad (29d)$$

Numerical calculation demonstrates that $M'(t)$ is smaller than $M_1(t)$ by a factor of 10^{-5} (magnitude of s/σ_1) which is consistent with the fact that $M'(t)$ is non-zero only if the terms of order s/σ_1 are included in solving the Euler equations above. In addition, inclusion of the first term in $Q_N(s)$ which is approximately of the order of magnitude of $(B - A)/A$ (10^{-5}) modifies the N -1 roots, which are computed by excluding the first term, by the same order of magnitude, and also introduces a new root which is smaller than the minimum of the N - 1 roots by a factor of 10^{-5}. This new λ root of course makes no significant contribution to $M_1(t)$, which is clear by inspection of (29), and therefore makes no significant contribution to the calculation of the present-day polar wander. The present analysis also demonstrates in a much more general manner that the approximations employed by *Peltier* [1982] and *Wu and Peltier* [1984] are entirely reasonable in the analysis of the present-day polar wander that is expected due to the glaciation-deglaciation cycle that has been a durable characteristic of the climate system for the last 900,000 years.

Perturbations of Inertia

To compute polar wander velocity and the variation of the axial rate of rotation, we need explicit expressions for I_{13}, I_{23}, and I_{33}. For the viscoelastic Earth models that we shall employ the total perturbation of inertia I_{ij} consists of the direct part I_{ij}^R resulting from the surface mass load, a part that is clearly independent of the rheological properties of the Earth model, and the part arising from the deformational response of the model to the surface load. The rigid part, I_{ij}^R, includes contributions from both the ice load and ocean load.

Since both the ice sheet and ocean components of the surface load are thin compared with the radius of Earth, it is therefore reasonable to treat this surface load as a layer of surface mass density $\sigma(\theta, \phi, t)$, where θ and ϕ are colatitude and longitude. The perturbations of inertia due to this surface load may then be computed using

$$I_{ij}^R(t) = \int\int \sigma(\theta,\phi,t)\,(a^2\delta_{ij} - x_i x_j)\,ds\ , \quad (30)$$

in which the surface integral is over the entire surface of the planet and a is the mean radius of the Earth. To evaluate (30), we expand the surface mass load $\sigma(\theta, \phi, t)$ in spherical harmonics as

$$\sigma(\theta,\phi,t) = \sum_{n=0}^{\infty}\sum_{m=-n}^{n}\sigma_{nm}(t)\,Y_{nm}(\theta,\phi)\ , \quad (31)$$

in which the spherical harmonics $Y_{nm}(\theta, \phi)$ are defined as

$$Y_{nm}(\theta,\phi) = P_{nm}(cos\,\theta)\,e^{-im\phi}\ . \quad (32)$$

The associated Legendre functions $P_{nm}(\cos\theta)$ are normalized such that the following orthogonality condition applies:

$$\int Y_{nm}(\theta,\phi)\,Y_{\ell k}^*(\theta,\phi)\,ds = 4\pi\,\delta_{nm}\,\delta_{\ell k}\ . \quad (33)$$

Substitution of (31) into equation (30), through the use of the orthogonality relation (33), then leads to the results

$$I_{13}^R(t) + i I_{23}^R(t) = -\left(\frac{32}{15}\right)^{1/2}\pi a^4\sigma_{21}(t)\ , \quad (34)$$

$$I_{33}^R(t) = -\frac{8}{3}\pi a^4\left[\left(\frac{1}{5}\right)^{1/2}\sigma_{20}(t) - 2\sigma_{00}(t)\right]. \quad (35)$$

To calculate $I_{13}^R(t)$, $I_{23}^R(t)$, and $I_{33}^R(t)$, we therefore need only the degree 2 expansion coefficients of the ice load and ocean load. The nature of the calculation of $I_{13}^R(t)$, $I_{23}^R(t)$, and $I_{33}^R(t)$ associated with the ice load will be described first. The latest deglaciation model ICE-4G of *Peltier* [1994] will be invoked to provide the detailed loading history associated with the ice sheets from LGM (last glacial maximum) to the

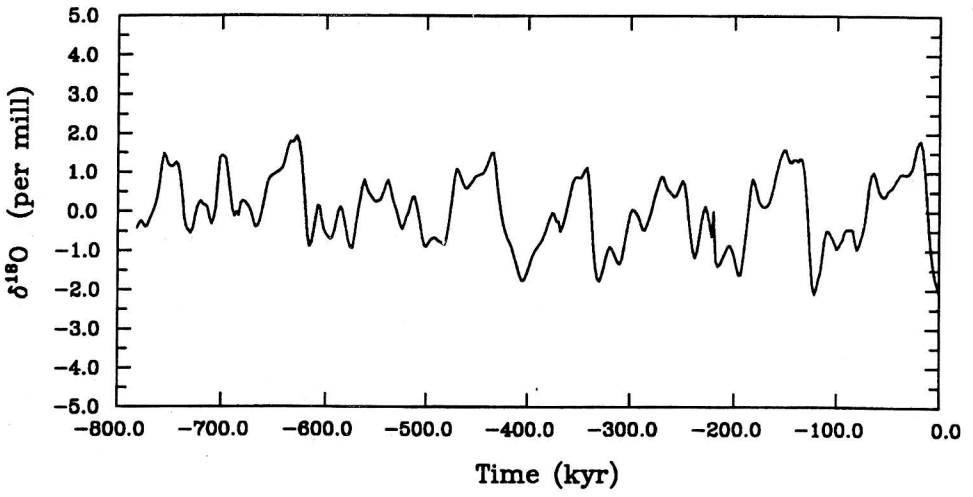

Figure 4. $\delta^{18}O$ time series based upon a stack of five deep-sea cores as described by *Imbrie et al.* [1984] and called SPECMAP stack. The $\delta^{18}O$ data provide tight constraints upon the Pleistocene history of ice volume fluctuations.

present-day. This model consists of thickness distributions for the main ice sheets at 1-kyr time intervals. Values of $I^R_{13}(t)$, $I^R_{23}(t)$, and $I^R_{33}(t)$ from 21,000 years ago to the present are calculated by performing spherical harmonic expansions of the data for ICE-4G. A sequence of representative maps of the time dependence in northern hemisphere projection for the ICE-4G model were discussed previously in connection with Plate 1. For times prior to the LGM, there exists no consensus model of ice loading history and we are obliged to make a number of approximations in order to construct a reasonably accurate model for the entire late Pleistocene period. *Wu and Peltier* [1984] employed a sawtooth function of time to approximate the ice loading history associated with the dominant 100-kyr glaciation-deglaciation cycle. This may not reflect with sufficient accuracy the short timescale fluctuations of ice sheet thickness, however, and in the present analysis we shall base our model of the pre--LGM loading history on the SPECMAP $\delta^{18}O$ record of *Imbrie et al.* [1984], shown on Figure 4, since the variations of $\delta^{18}O$ are directly related to the variation of the volume of the ice sheets [*Shackleton*, 1967]. Such a model is expected to be considerably more accurate than the sawtooth approximation employed previously. To create a complete space--time model of the surface ice load from 780,000 years ago to LGM using the $\delta^{18}O$ record, we assume that at all times prior to LGM the ice distribution was the same as that at LGM but that each ice sheet had a thickness which is a linear function of the $\delta^{18}O$ anomaly. This approximation clearly ignores the impact of change in surface area of the ice sheets as they grow and decay through the late Pleistocene cycle of glaciation-deglaciation. As discussed by *Peltier and Jiang* [1994], however, this approximation only slightly exaggerates the projection of the ice load onto the spherical harmonics of degree 2, and the impact on the calculation of perturbations of inertia will be skewed only by an exaggeration of the extent of glacial isostatic equilibrium predicted to obtain at LGM. Since ICE-4G was in fact constructed on the basis of the assumption of precise isostatic equilibrium at LGM it is expected that this treatment of the prehistory will lead to a more self-consistent analysis than that employed by *Mitrovica and Peltier* [1993a] whose treatment leads to the prediction of significant disequilibrium at LGM. Once the space-time model of the ice load has been constructed in this way, its expansion in spherical harmonics with time dependent coefficients is clearly straightforward.

To compute the perturbations of inertia associated with the ocean load, we must first consider the variations of relative sea level induced by ice sheet melting on the viscoelastic Earth. As the thickness of the ice sheets changes, the ocean load changes not only so as to conserve the total mass of the ocean-ice system but also so as to ensure that the ocean surface remains a gravitational equipotential surface at all times. Taking the ice loading history as input data, the complete solution to the general sea level equation [e.g. *Peltier et al.*, 1978] is required to provide a gravitationally self-consistent history of ocean loading. The method we shall use to solve the sea level equation (1) in the analyses to be presented here is that described by *Mitrovica and Peltier* [1991] based upon a spherical harmonic expansion technique. Given the time dependent ice load, from 780,000 years ago to the present-day, the solution of the sea level equation delivers the time dependent functional form of the ocean load over the same period of time in terms of time dependent coefficients of the spherical harmonic expansion of relative sea level. The ocean load contributions to the required time series for $I^R_{13}(t)$, $I^R_{23}(t)$, and $I^R_{33}(t)$ are then computed according to (34) and (35).

Figure 5 displays the time series for $I^R_{13}(t)$, $I^R_{23}(t)$ and $I^R_{33}(t)$ from LGM to the present-day, based upon the deglaciation model ICE-4G [*Peltier*, 1994]. The zero of time in Figure 5 is set to correspond to the present-day. The values of $I^R_{13}(t)$, $I^R_{23}(t)$, and $I^R_{33}(t)$ at LGM were previously estimated by *Wu and Peltier* [1984] who modelled the main ice sheets as circular disk loads. Table 1 lists the results for $I^R_{13}(t)$, $I^R_{23}(t)$, and $I^R_{33}(t)$ obtained in the present analysis and those obtained previously by *Wu and Peltier* [1984] (due to an error in *Wu and Peltier* caused by the use of the wrong sign for the Legendre polynomial $P^1_2(\cos\theta)$ in the expressions for the perturbations of inertia, the values for $I^R_{13}(t)$, $I^R_{23}(t)$, and $I^R_{33}(t)$

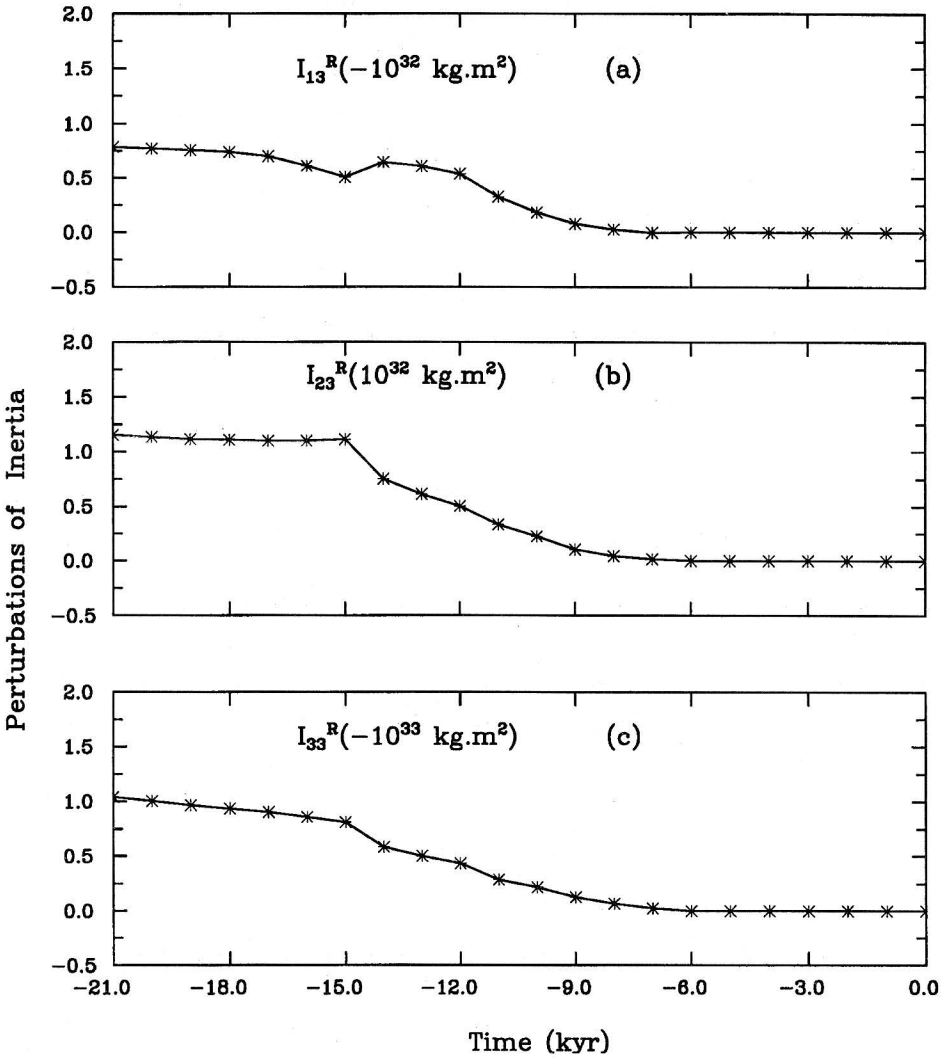

Figure 5. Perturbations of the three principal moments of inertia caused by the direct effect of the surface load from LGM to the present-day computed from the deglaciation model of *Peltier* [1994]. The zero of time is taken to be the present day. The radial viscosity profile to which the computed perturbations correspond is characterized by a 120 km lithosphere, an upper mantle of viscosity 10^{21} Pa s, and a lower mantle with a viscosity of 2 x 10^{21} Pa s.

have been revised for this earlier analysis to be -1.407 x 10^{32}, 2.160 x 10^{32} and -7.842 x 10^{32}, respectively). As will be clear from Table 1, in comparison with the results obtained in the previous analyses of *Wu and Peltier*, the magnitude of I_{13}^R in the present analysis is reduced by 43%, that of I_{23}^R by 48%, while the magnitude of I_{33}^R is increased by 38%. Figure 6 shows time series for $I_{13}^R(t)$, $I_{23}^R(t)$, and $I_{33}^R(t)$ from 780,000 years ago to the present-day computed from the ice loading history constructed as discussed above and an ocean loading history determined by employing this forcing function to construct a time dependent solution to the sea level equation. These time series provide the perturbations of the elements of the inertia tensor over the glaciation--deglaciation cycle that are required to compute both polar wander velocity and the secular variation in $\dot{J}_2$. Of course, the time series shown in Figure 6 (and in Figure 5) have been obtained with a particular choice for the radial viscoelastic structure, in this case the viscosity of the upper mantle has been fixed to the value of 1 x 10^{21} Pa s, the viscosity of the lower mantle to the value of 2 x 10^{21} Pa s and the lithospheric thickness to 120 km. For each variation of this structure that is of interest a new solution to the sea level equation must be constructed in order to generate a self-consistent model for the variations of the elements of the inertia tensor.

Results: Gravitationally Self-Consistent Polar Wander and Nontidal Acceleration

In order to illustrate the results delivered by the above described gravitationally self-consistent theory, we have first computed the present-day polar wander velocity (both magnitude and direction) for a sequence of viscoelastic Earth models that differ from one another only in the viscosity of the lower mantle ν_{LM} (below a depth of 660 km). The radial elastic structure of this suite of models, including the density field, is fixed to that of (PREM) [*Dziewonski and Anderson*, 1981], the viscosity of the upper mantle is fixed to the value ν_{UM} = 1 x 10^{21} Pa s, and the thickness of the lithosphere is fixed to the value of 120 km. Figures 7a and 7b show the

Table 1. Values of I^R_{13}, I^R_{23}, and I^R_{33} at the Last Glacial Maximum (LGM)

	I^R_{13} (10^{32} kg m^2)	I^R_{23} (10^{32} kg m^2)	I^R_{33} (10^{32} kg m^2)
Wu and Peltier [1984]	-1.407	2.160	-7.842
This analysis	-0.804	1.129	-10.783
Difference	43	48	38

magnitude and direction of the polar wander velocity computed for three of these viscoelastic Earth models using the perturbations of inertia that were illustrated for one viscoelastic model in Figure 6. The origin in time is set to be the present-day. On Figure 7a the computed time dependent magnitude of the polar wander velocity is shown along with the observed value of the present-day polar wander speed. The observed present day polar wander speed, which ranges from 0.8°/Myr years to 1.1°/Myr years is marked by the square in Figure 7a. As clear from Figure 7a, the model which best fits the observed polar wander speed has a viscosity of the lower mantle near $\nu_{LM} \simeq 2 \times 10^{21}$ Pa s. As the value of ν_{LM} increases, the predicted polar wander speed decreases, and vice versa. Figure 7b presents the polar wander angle prediction for the same three illustrative models. The negative value of the angle corresponds to west longitude. The predicted direction of polar wander for all of these models is in good agreement with the observed direction of polar wander, with the differences in the angle between the predictions being less than one degree. The reason for this weak sensitivity of the predicted direction of polar wander upon the viscosity model is that the direction of polar wander is almost entirely determined by the distribution of the ice sheets and is not sensitive at all to the rate of isostatic adjustment which dominates the prediction of the present-day polar wander speed. It is quite clear from the analysis of *Wu and Peltier* [1984] that the direction of polar wander velocity is simply determined by the ratio of the value of I^R_{13} at LGM to that of I^R_{23} to the extent that the

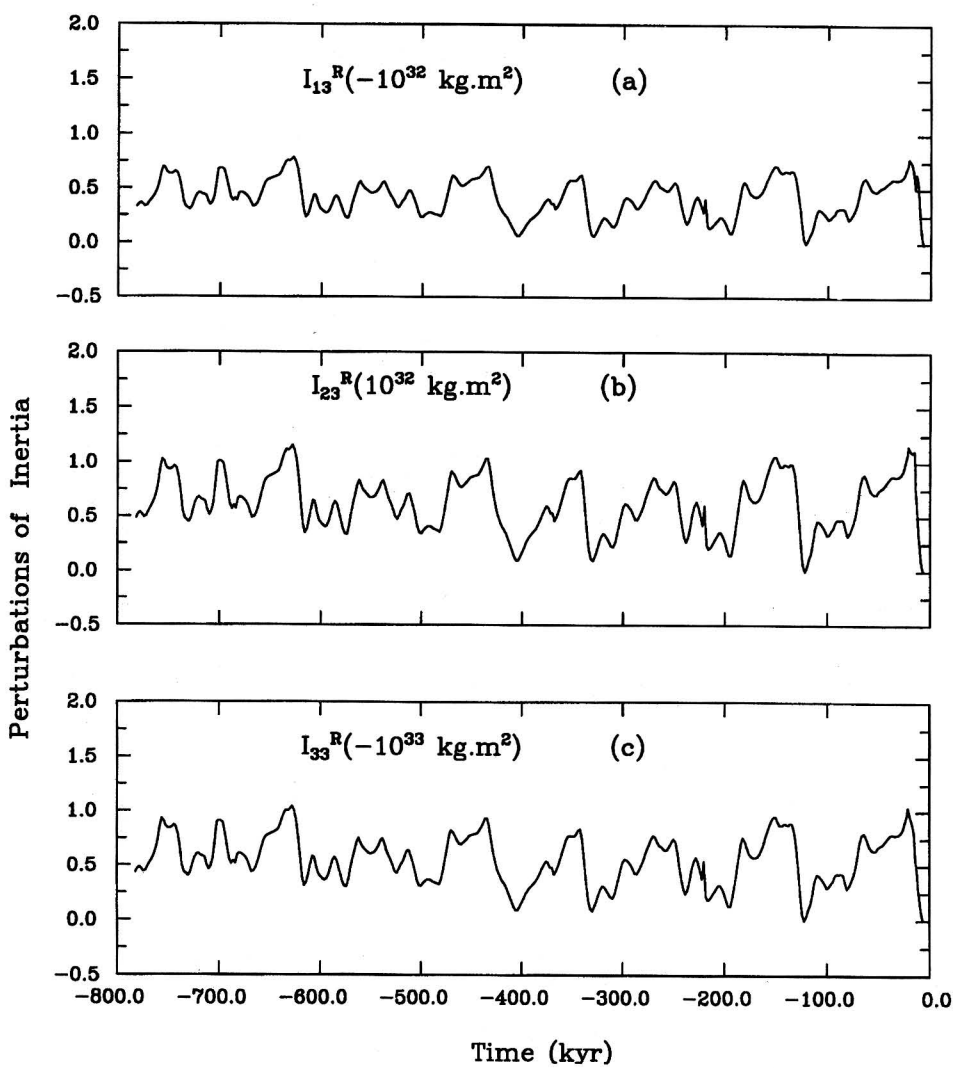

Figure 6. The perturbations of the three principal moments of inertia from 780,000 years ago to the present-day caused by the direct effect of the surface load. The zero of time is taken to be the present-day. The major cycles in I^R_{13}, I^R_{23}, and I^R_{33} correspond to the glaciation-deglaciation cycles, visible in the $\delta^{18}O$ data shown on Figure 4.

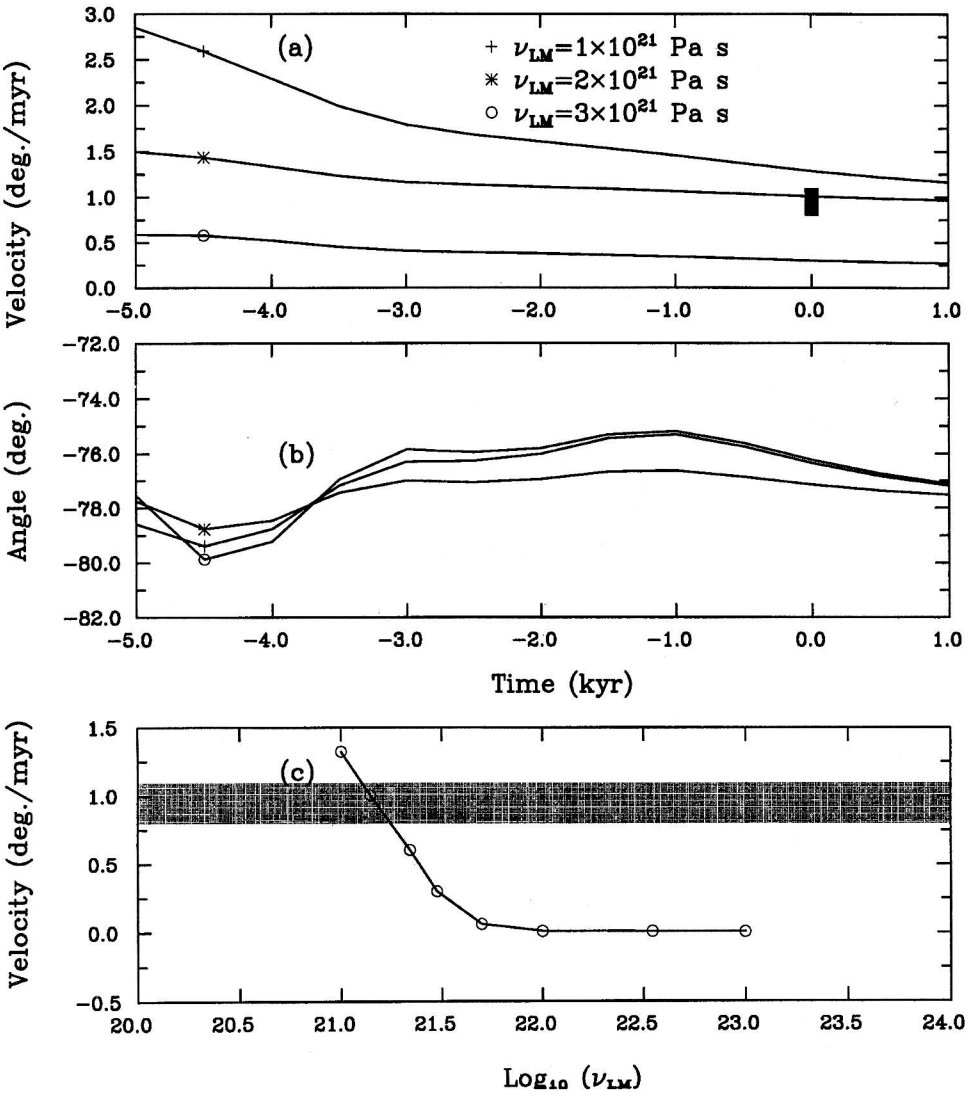

Figure 7. The magnitude and angle of polar wander velocity computed for the three viscoelastic Earth models whose values of the lower mantle viscosity ν_{LM} are illustrated. The range of the observed values of polar wander speed is marked by the square.

sawtooth approximation to the loading history may be considered adequate. Nevertheless, any model developed to fit the observed polar wander speed must also predict the observed direction of polar wander within the observational error. Figure 7c shows the computed magnitude of present day polar wander velocity as a function of the viscosity of the lower mantle, and the hatched region on the same figure denotes the range of observed present day polar wander speed. This monotonic change of the predicted present-day polar wander speed as a function of lower mantle viscosity (which appears to be discordant with the recent report by *Spada et al.* [1992]) is extremely important since the observed polar wander speed is thereby shown to provide an unambiguous constraint on the viscosity of this region if the viscosity of the upper mantle may be assumed known. The nature of this constraint is therefore strikingly different from that delivered by the observed nontidal acceleration of rotation which, as we will discuss further below, may be fit either by models with weak viscosity contrast between upper and lower mantle or with high contrast.

Since the prediction of the present-day polar wander depends on the loading history to which the system is subject, an interesting question concerns the issue as to how important is the duration of the prehistory needed to obtain a reasonably accurate prediction of the present-day signal. We have therefore carried out a numerical experiment in which the predictions of the present-day polar wander for three models are computed by applying different loading histories to the system, and the results of these experiments are listed in Table 2. It is clear by inspection of the entries in Table 2 that approximately 70% of the predicted magnitude of polar wander velocity is determined by the loading history associated with the last deglaciation event. This emphasizes the extreme importance of having an accurate deglaciation model in calculations of the present-day polar wander. As might be expected based upon our previous comments, the direction is essentially independent of these variations of the loading history. The relative differences between the magnitude computed from a loading history of 600,000 years and that from a loading history of 700,000

Table 2. Speed and Direction of Polar Wander for Three Illustrative Viscoelastic Models

Time, kyr	ν_{LM}= 1 x 10^{21}		ν_{LM}= 1 x 10^{21}		ν_{LM}= 1 x 10^{21}	
21	0.989	-75.9	0.737	-76.9	0.254	-76.5
200	1.078	-76.1	0.822	-77.0	0.263	-76.1
300	1.139	-76.2	0.878	-77.1	0.271	-76.1
400	1.191	-76.2	0.926	-77.1	0.278	-76.1
500	1.228	-76.3	0.959	-77.1	0.286	-76.2
600	1.261	-76.3	0.987	-77.1	0.293	-76.2
700	1.285	-76.4	1.006	-77.2	0.299	-76.2

Direction of polar wander is given in degrees longitude, negative implying west of Greenwich. The three models were computed on the basis of the assumption of different durations for the loading history that is indicated by the time before present at which integration is initiated.

years are 1.87% for ν_{LM} =1 x 10^{21} Pa s, 1.89% for ν_{LM} = 2 x 10^{21} Pa s, and 2.05% for ν_{LM} = 3 x 10^{21} Pa s. In comparison with the observational error of the polar wander speed (about 15%), the result computed using the loading history of 700,000 years is clearly acceptable. The results shown on Figure 7 are computed by using the complete SPECMAP loading history that extends from approximately 780,000 years ago as discussed in the preceding section.

Based upon the analyses presented in this section, we conclude that the observed polar wander velocity is quite simply explained as a consequence of ongoing glacial isostatic adjustment following the last deglaciation event of the current ice age. In order to best fit both magnitude and direction of polar wander, the model with the viscosity of the lower mantle $\nu_{LM} \simeq 2 \times 10^{21}$ Pa s is preferred when the viscosity of the upper mantle is fixed to the value of 10^{21} Pa s. This is an extremely important result as it demonstrates a global self-consistency of the analysis performed with the ICE-4G deglaciation model in the sense that the model was inferred by fitting postglacial relative sea level histories from sites that were once ice covered with precisely the same model of the radial viscosity profile of the mantle. Before the implications of this analysis are entirely accepted, however, we are clearly obliged to demonstrate that the same model is capable of explaining the observed secular variation in $\dot{J}_2$ that is related to $\dot{m}_3$ in the way described by (22). Any model of the radial viscoelastic structure which fits the polar wander observation must also fit the observed $\dot{J}_2$ within the observational errors, if it is to be considered an acceptable model.

In order to express $\dot{m}_3$ in terms of I^R_{33}, we must solve (7c) with $\tilde{\psi}_3$ being given by (8c) in which $I_{33}(t)$ may be expressed as the convolution of $I^R_{33}(t)$ with $k^L_2(t)$. In the time domain, the load Love number k^L_2 of degree 2 [*Peltier*, 1974, 1976, 1985] is expressible, when the relaxation spectrum is discrete, as

$$k_2^L(t) = k_2^{LE}\,\delta(t) + \sum_{j=1}^{N} r_j e^{-s_j t}. \tag{36}$$

Equation (7c) may be easily solved in the time domain due to its simple structure. Substituting (36) into (7c) and then integrating, we may write $\dot{m}_3$ as

$$\dot{m}_3(t) = -\frac{1}{C}\left[D_1 \dot{I}^R_{33}(t) + \sum_{j=1}^{N} r_j I^R_{33}(t) - \sum_{j=1}^{N} r_j s_j I^R_{33}(t) * e^{-s_j t} \right]. \tag{37}$$

According to the definition of J_2, $\dot{J}_2$ is identical to $\dot{m}_3$ within a constant multiplier [*Wu and Peltier*, 1984], and this relation is simply

$$\dot{J}_2(t) = -\frac{3C}{2a^2 M}\,\dot{m}_3(t) \tag{38}$$

in which M is the mass of Earth.

In Figure 8a, we show the results obtained by computing variations in $\dot{J}_2$ for the same three models employed previously in illustrating the results obtained from the calculation of polar wander velocity. Three observed values of $\dot{J}_2$ are shown in Figure 8a. Among them, two values, which are (-3.5 ± 0.3) x 10^{-11} yr^{-1} and (-2.5 ± 0.3) x 10^{-11} yr-1, have been determined on the basis of satellite geodesy by *Yoder et al.* [1983] and by *Cheng et al.* [1989], respectively. The third value shown, which is (-3.5 ± 0.8) x 10^{-11} yr^{-1}, is that obtained by *Stephenson and Morrison* [1995] on the basis of the analysis of records of solar and lunar eclipses in the period 700 B.C. to 1600 A.D. The results shown on Figure 8a indicate that the viscosity of the lower mantle required to fit the observed value of $\dot{J}_2$ is the same value which also fits the observation of polar wander. Unfortunately, this fit is not similarly unambiguous since, as shown in Figure 8b, there is another range of lower mantle viscosity which also provides a fit to the $\dot{J}_2$ observation, that centered upon the value 10^{23} Pa s. Both on the basis of solutions to the forward problem for postglacial sea level history [*Peltier*, 1974, 1976, 1982; *Peltier et al.*, 1986] and solutions to the inverse problem [*Mitrovica and Peltier*, 1993, 1995], it is, however, clear that the viscosity of the upper part of the lower mantle is bounded above by the value 2 x 10^{21} Pa s if the viscosity of the upper mantle is fixed to 1 x 10^{21} Pa s. This constraint, along with the previously discussed constraint provided by polar wander speed, therefore entirely suffices to rule out the high-viscosity solution for the lower mantle when the viscosity of the upper mantle is fixed to 10^{21} Pa s.

Since the sea level data have no resolving power for viscosity below approximately 1400 km depth, and since the formal inversions of postglacial rsl data strongly suggest that the viscosity of the mantle remains equal to its "low" upper mantle value to a depth near 1400 km, it is clearly of great interest to enquire as to what the rotational data would imply concerning the viscosity of the deepest part of the lower mantle if this rsl constraint were invoked to fix the remainder of the structure. Furthermore, according to *Forte and Peltier* [1987, 1989, 1991], and to *Pari and Peltier* [1995], inferences of the viscosity profile based upon convection-related constraints such as the nonhydrostatic geoid, derived by application of models constrained by seismic tomography, require the viscosity of the lower half of the lower mantle to be significantly higher than 2 x 10^{21} Pa s. What we are interested in here is whether we might

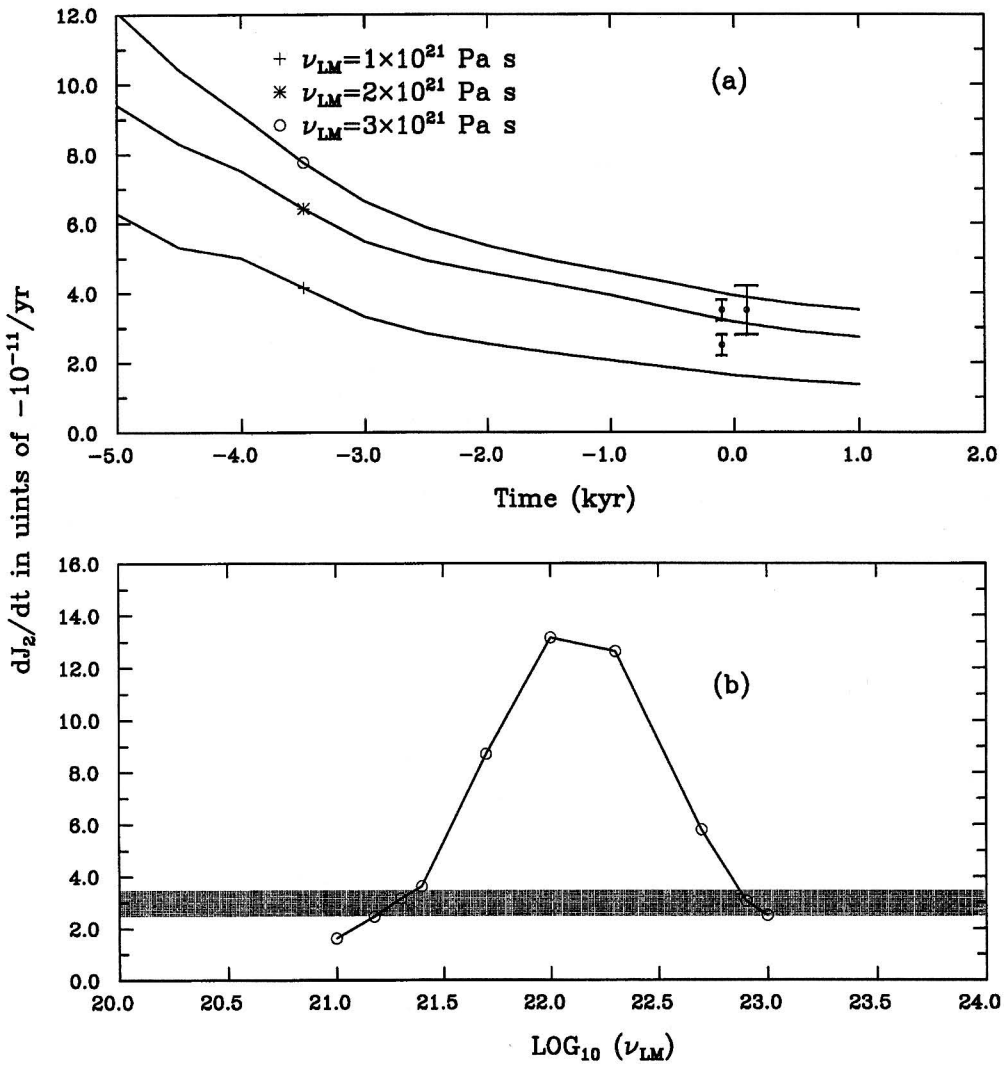

Figure 8. (a) Secular variation in $\dot{J}_2$ for the same three models as employed for the analysis of polar wander speed in Figure 7. Observations illustrated are (-3.5 ± 0.8) x 10^{-11} [*Stephenson and Morrison*, 1994], (-3.5 ± 0.3) x 10^{-11} yr^{-1} [*Yoder et al.*, 1983], and (-2.5 x 0.3) x 10^{-11} yr^{-1} [*Cheng et al.*, 1989]. (b) The predicted variation of $\dot{J}_2$ for the present-day as the function of the viscosity of the lower mantle.

continue to fit both the polar wander and $\dot{J}_2$ data unambiguously if we maintain the viscosity of the upper part of the lower mantle from 660 km to 1400 km to be equal to the value of the upper mantle but introduce much higher values of viscosity in the region below 1400 km depth.

To perform the required numerical experiments, we therefore introduce a layer of high viscosity, comparable to the value required to fit the observed nonhydrostatic geoid in terms of a tomography-based convection model, for the lower part of the lower mantle below 1400 km depth. For the purpose of this new sequence of experiments we also fix the viscosity of the upper mantle and of the upper part of the lower mantle to the value 1 x 10^{21} Pa s. A sequence of models which differ only in the viscosity of the lower part of the lower mantle ν_{LLM} are then employed to recompute the present-day polar wander speed and secular change of J_2, and the results are shown in Figure 9. Both the present-day predicted polar wander speed and value of $\dot{J}_2$ are plotted as a function of the viscosity of the lower part of the lower mantle ν_{LLM}. The solid areas denote the observational constraints. As is clear on the basis of inspection of Figure 9a, in order to fit the observed polar wander speed the required value of ν_{LLM} lies in the range 12-14 x 10^{21} Pa s, an increase by a factor of 6 to 7 in comparison with the value of ν_{LM} inferred on the basis of models in which the entire lower mantle is assumed to have the same constant viscosity. The upper bound of this allowed range is close to that obtained by *Forte and Peltier* [1987, 1989, 1991] by fitting the observed nonhydrostatic geoid using a tomography based convection model, and more accurately reconfirmed by *Pari and Peltier* [1995] using the same methodology. To fit the observed $\dot{J}_2$, the required values of ν_{LLM} are between 13 x 10^{21} and 15 x 10^{21} Pa s, a result which is clearly consistent with the result determined on the basis of the fit to polar wander speed. Since the variation of J_2 is actually quite sensitive to the response of the lower part of the lower mantle to the glaciation-deglaciation process, as illustrated by the Freché kernel for $\dot{J}_2$ shown in Figure 10a, observations of $\dot{J}_2$ are important to constraining the viscosity of the lower part of the lower mantle where the sea level data have little

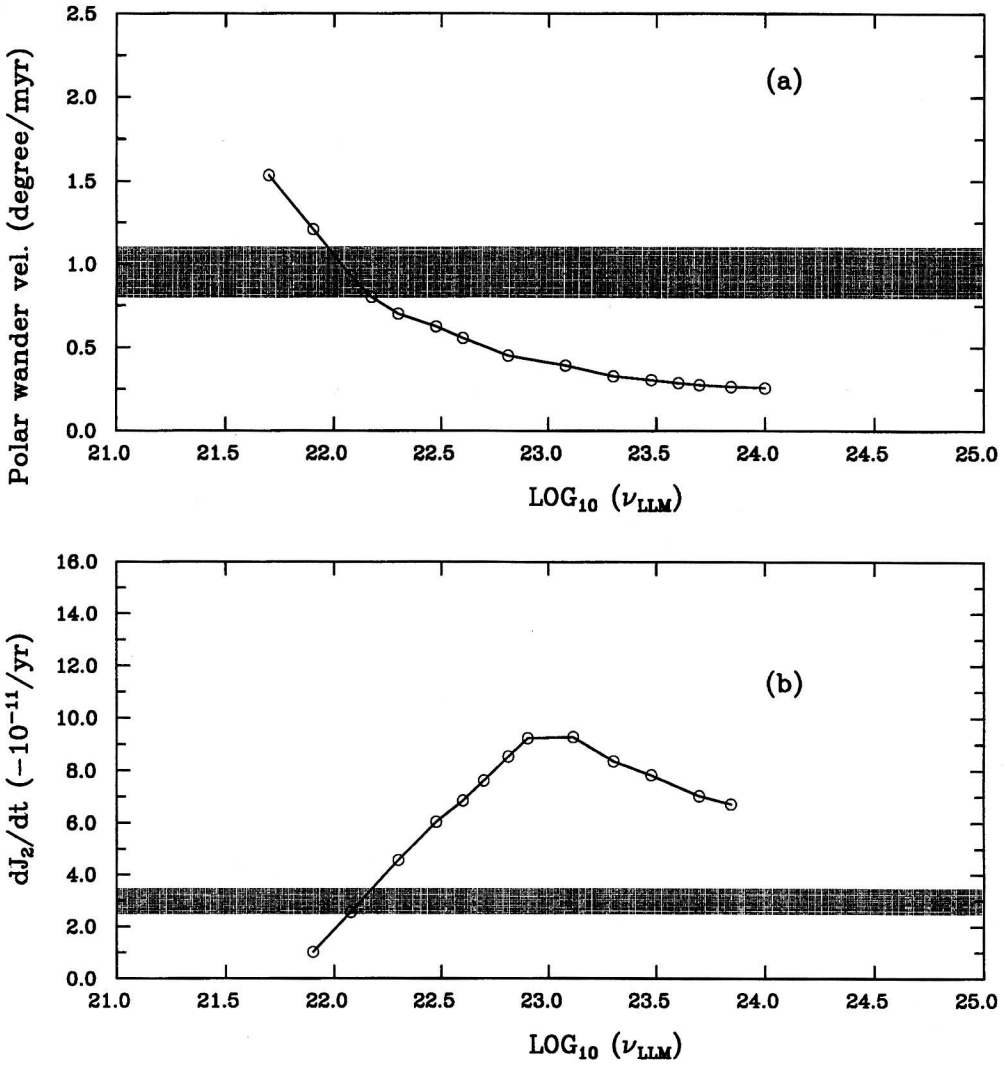

Figure 9. The predicted polar wander speed and value of $\dot{J}_2$ for the present day as the function of the viscosity of the lower part of the lower mantle ν_{LLM}. The hatched areas represent the observed ranges of the polar wander speed and $\dot{J}_2$. (a) Polar wander speed for the present-day. (b) Secular variation of J_2 for the present day.

resolving power. Of special interest here is the fact that the second viscosity root is completely ruled out when the depth at which the increase in viscosity is introduced is moved from 660 km to 1400 km.

By way of rounding out this discussion and more firmly connecting it to the ongoing effort involving formal inversion of the data of post-glacial rebound, we show in Figure 10a the Fréchet kernels $FK(r)$ for both the non-tidal acceleration of rotation and $\dot{J}_2$ observables. These kernels, computed on a starting model with lithospheric thickness L = 120 km, upper mantle viscosity $\nu_{UM} = 10^{21}$ Pa s and lower mantle viscosity $\nu_{LM} = 2 \times 10^{21}$ Pa s, describe the sensitivity of either observational datum D to variations in the mantle viscosity profile as:

$$\delta D = \int_a^b FK(r)\, \delta \ell n \nu(r)\, r^2\, dr . \qquad (39)$$

The $FK(r)$ are therefore functional derivatives of the "data" with respect to the model parameter. Given these Fréchet kernels it is rather straightforward to converge onto a maximum likelihood estimate of the mantle viscosity profile $\nu(r)$ using the methodology of Bayesian inferences [e.g., *Tarantola and Valette*, 1982a,b).

In Figure 10*b* we illustrate the results that are obtained when the Bayesian methodology is employed to simultaneously invert the Fennoscandian relaxation spectrum derived by McConnell [1968] and recently inverted by *Mitrovica and Peltier* [1993], the site specific relaxation time data for Hudson Bay described by *Mitrovica and Peltier* [1985] and the rotational data that have been discussed herein. The Figure shows the results of three such inversions, respectively for cases (model 1) in which the rotational data are assumed to be unbiased by any significant influence of present day melting of polar ice [e.g., *Peltier*, 1988] and for scenarios in which it is assumed that polar ice is melting such as to deliver a contribution to the present day rate of relative sea level rise of either 0.5 mm yr^{-1} or 1.0 mm yr^{-1} (models II and III respectively). Inspection of the a-posteriori models delivered by the Bayesian iterative procedure shows that the models are all characterized by significant

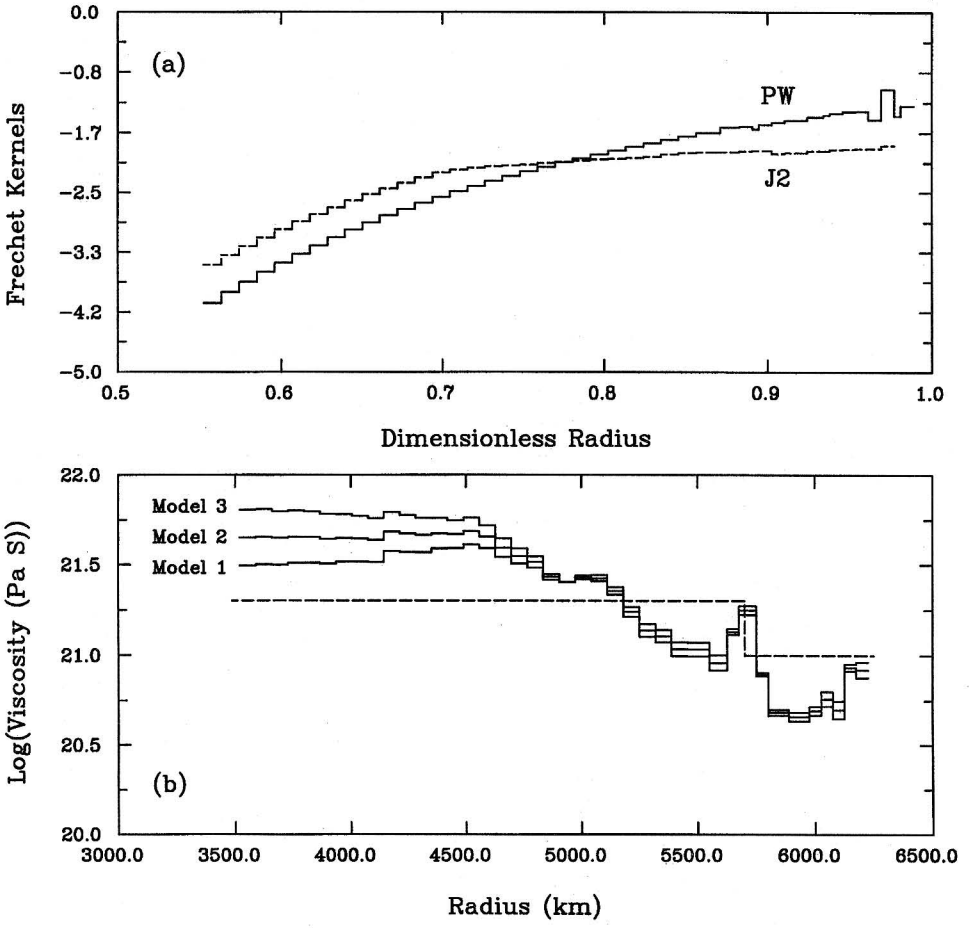

Figure 10. (a) Fréchet kernels for $\dot{J}_2$ and for polar wander speed as a function of the dimesionless radius. These kernels have been caculated using the ICE-4G deglaciation model and the Earth model with $\nu_{LM} = 2 \times 10^{21}$ Pa s. (b) Viscosity depth profiles obtained by formal inversion of relative sea level data both excluding (model I) and including the influence of the bias due to the present day melting of land ice. Model II assumes present day melting of 0.5 mm yr^{-1} whereas model III assumes 1.0 mm yr^{-1}.

increases of mantle viscosity with depth, the more so the larger the bias on the observations due to the present day melting of land ice. The viscosity of the upper part of the lower mantle is now formally fixed to a value close to the Haskell number of 10^{21} Pa s, the viscosity of the upper mantle to a value which is a factor 2 or 3 lower than this, and the viscosity of the lowermost mantle to a value that is indeed significantly higher. The precise value of the viscosity in the lowermost mantle is however quite sensitive to the existence of any influence due to the ongoing melting of polar ice and mountain glaciers. The sense of this influence is such as to significantly increase the value of the viscosity of the deepest mantle that is preferred by the totality of the data. More detailed discussions of the results of these simultaneous inversions will be found in discussions to be published elsewhere.

Discussion and Conclusions

The analyses of Earth's rotational response to the 100-kyr glaciation-deglaciation cycle of the late Pleistocene presented herein have clearly demonstrated the quality of the constraint on deep mantle viscosity that such data provide. Their utility in this regard is clearly due to the fact that the rotational response depends solely upon the spherical harmonic constituents of degree 2 in the deformation of planetary shape that is caused by the loading and unloading process. Such long horizontal wavelengths have the greatest possible sensitivity to the viscosity in the deepest part of the lower mantle. It will therefore be useful to reiterate here the main arguments concerning the implications of these data that have been presented in the main body of this paper.

First, concerning the theory on the basis of which the polar wander response to the glacial cycle must be calculated, we have herein developed the complete analysis for a gravitationally tri-axial Earth model which supersedes the biaxial theory previously elaborated by *Peltier* [1982] and *Wu and Peltier* [1984]. On the basis of this more general theory we have demonstrated explicitly that the error previously committed through the use of a biaxial theory was extremely small, of order a fraction of a percent at most in polar wander speed. As discussed in detail in those earlier papers the mathematical form of the polar wander prediction is completely different from that for the nontidal acceleration of rotation. Nonzero present day polar wander speed is

predicted only because of the multiplicity of modes of viscous-gravitational relaxation that are characteristic of a radial viscoelastic model of the planetary interior. The same is not the case for the non-tidal acceleration, a datum that could be adequately reconciled using a homogeneous viscoelastic model. This difference in the theoretical structure of the solutions for these two forward problems for the different components of the rotational response leads to a striking difference in the variation of the magnitude of the response as a function of the radial viscosity profile in the planetary mantle. The most important contribution of the present paper is in providing a rather detailed exploration of this differential sensitivity to the radial variation of viscosity.

Briefly stated, for models of the mantle with realistic radial elastic structure determined seismically and with simple two-layer viscosity stratification the following is found to be the case. Fixing the viscosity of the shallower layer to the nominal viscosity value of 10^{21} Pa s initially inferred by *Haskell* [1935], the polar wander speed observation allows only one value of the viscosity of the deeper layer. When the lower boundary of the upper layer is taken to be located at 660 km depth, then this datum constrains the viscosity of the lower layer to be near 2×10^{21} Pa s, insignificantly different from the viscosity of the upper layer. The nontidal acceleration observation, on the other hand, may be fitted by either one or the other of two distinct viscosity values for the lower layer. One of these "roots" is identical to the single value of the lower mantle viscosity required to fit polar wander speed. The second is approximately 2 orders of magnitude higher. That the polar wander speed observation could be invoked to uniquely constrain the upper mantle-lower mantle viscosity contrast, and thus rule out the higher-viscosity root allowed by the nontidal acceleration, has been demonstrated only very recently [*Peltier and Jiang*, 1994]. This paper is the first to explore the detailed consequences of this result.

When taken in conjunction with the constraints upon the radial profile of mantle viscosity that are delivered by postglacial relative sea level variations, the implications of the rotational data upon which we have focused here become especially important. It is well known on the basis of solutions to the forward problem for such observations [e.g., *Peltier* 1974; *Cathles*, 1975; *Peltier et al.*, 1986; *Peltier*, 1989] that these data rule out the occurrence of any substantial increase in the large spatial scale radial average value of the viscosity of the mantle across the 660-km discontinuity that bounds the transition zone from below. This result, which has recently been reconfirmed through the application of formal inverse theory to the same observational data [*Mitrovica and Peltier*, 1993b, 1995] is also compatible with the independent inference based upon the rotational constraints upon which we have focused in this paper. Although a number of alternative analyses of small subsets of the relative sea level data have recently been presented which conflict with these inferences, these analyses [e.g., *Nakiboglu and Lambeck*, 1980; *Han and Wahr*, 1995] have been sketchy at best as their authors were unable to reconcile the complete set of relative sea level data from Hudson Bay. In particular, neither of these analyses were able to satisfy the rsl data from the majority of sites which are characterized by short relaxation times from 3 kyr to 5 kyr. A detailed discussion of the problems with these analyses has been provided by *Mitrovica and Peltier* [1993b, 1995]. As discussed by *Peltier* [1982] (and subsequent papers), it is the exponential relaxation time constant that is characteristic of the postglacial rebound process at once ice-covered sites, in the time since deglaciation was complete, that is almost exclusively determined by mantle rheology. When this feature of the rebound process at individual sites is employed to parameterize the data, a formal theory of inference entirely rules out the plausibility of the high-viscosity contrast model suggested in these conflicting analyses.

The results that we have obtained through the application of formal inverse methods to the relative sea level data demonstrate that these data have significant resolving power only to depths of 1200-1400 km, even when rsl data from the large horizontal scale uplift of the Hudson Bay region are employed [*Mitrovica and Peltier*, 1995]. The rsl data from this region require that the viscosity of the mantle remain close to the value of 10^{21} Pa s to depths of this order. In order to accommodate the rsl constraint in the inversion of the rotational observations we have investigated the predictions of a further series of two-layer mantle viscosity profiles in which the depth to the lower boundary of the upper layer is shifted downward to 1400 km. Employing the rotational data to constrain the viscosity of this deepest part of the lower mantle we then infer a value between 1.2 and 1.5 x 10^{22} Pa s to be characteristic of this region. For this sequence of models both the polar wander speed and nontidal acceleration data again agree on the value of the viscosity of this deepest region of the mantle and furthermore the previous ambiguity of interpretation of the nontidal acceleration is removed [see also *Yuen and Sabadini*, 1985], there no longer being two possible values for the viscosity contrast between layers that will equally well reconcile the data.

This solution to the problem of the radial variation of mantle viscosity has much to recommend it, in our view, for reasons that extend well beyond the rather narrow confines of the postglacial rebound data on the basis of which our model has been derived. First, there is the issue of the compatibility of the postglacial rebound constraints on mantle viscosity and those which have been forthcoming recently based upon models designed to fit nonhydrostatic geoid anomalies. Such models employ constraints from seismic tomographic imaging to infer the three-dimensional variation of density within the mantle and a convection model to infer the contribution of dynamic tomography to the geoid height field. Such models make predictions of nonhydrostatic geoid anomalies that are extremely sensitive to the radial variation of viscosity [e.g. *Richards and Hager*, 1984; *Ricard et al.*, 1989; *Forte and Peltier*, 1987, 1989, 1991; *Corrieu et al.*, 1995; *Pari and Peltier*, 1995; *Peltier et al.*, 1995]. In the context of two-layer models of the radial stratification of mantle viscosity and with the lower boundary of the upper layer placed at a depth of 660 km these data have often been construed to require a viscosity increase across this horizon by at least a factor of 30. As very clearly demonstrated in the papers based upon the theory of Forte and Peltier, most recently discussed by *Pari and Peltier* [1995], it has however been shown that the radial profile of mantle viscosity that is inferred on the basis of nonhydrostatic geoid data is highly nonunique. In particular, these analyses demonstrate that if a thin low-viscosity layer were to be located just above the 660-km seismic discontinuity, then the nonhydrostatic geoid

data are well reconciled by models in which the viscosity of the upper part of the lower mantle is little different from the average viscosity of the upper mantle. Such models are entirely compatible with the postglacial rebound constraints and also fully satisfy the nonhydrostatic geoid data if the viscosity of the lower part of the lower mantle is significantly higher than that of the shallower region.

The analyses presented herein and by *Pari and Peltier* [1995] therefore suggest a highly plausible means whereby the previously assumed discrepancy between convection timescale and postglacial timescale inferences of the depth dependence of mantle viscosity may be reconciled. If in the interpretation of the postglacial rebound data we simply shift the boundary below which the viscosity of the mantle increases from the depth of the 660-km discontinuity to a depth near or below 1400 km, then the rotational data discussed herein require that the viscosity of the deeper layer increase from a value near 10^{21} Pa s to a value near 1.5 x 10^{22} Pa s, that is to say by approximately one order of magnitude. It is extremely important to note that models of this kind have previously been suggested as being optimal two-layer models for the reconciliation of nonhydrostatic geoid anomalies using tomography based convection models [*Forte and Peltier*, 1987, 1991]. As recently discussed by *Pari and Peltier* [1995] such models are able to provide an extremely satisfactory reconciliation of the nonhydrostatic geoid data when a sharply confined in radius and perhaps dipolar variation of viscosity is introduced across the 660-km discontinuity. If this localized structure consists of a thin low viscosity region above 660-km depth (and a perhaps equally thin high-viscosity region below 660-km depth), then it is essentially invisible to postglacial rebound data. As demonstrated explicitly by *Pari and Peltier* [1994] such models provide very high reduction of nonhydrostatic geoid variance. Alternatively and in equal accord with the postglacial rebound data is a model in which the entire upper mantle is somewhat softer than the top of the lower mantle (say by a factor of 4 or so; i.e. near the value of 4 x 10^{20} Pa s) with somewhat further enhanced softening in a thin layer above the 660 km discontinuity.

Clearly, the issue of the uniqueness of such models of the internal viscosity structure is important, and this is an issue which we have begun to address through formal inversions that employ the combined data of postglacial rebound and mantle convection. Further results from these formal inversions will be reported in due course. Also of great interest and concern is the question as to the role that lateral variations of viscosity may play, both in the context of convection- related and postglacial rebound-related observations. Although some recent progress has been made in incorporating the influence of such variations into models of the former process [*Forte and Peltier*, 1994], the available analyses are very much of a preliminary nature and much remains to be accomplished in this area.

What we have achieved by the analyses reported herein is the demonstration that it is in fact possible to reconcile both postglacial rebound and convection-related observations with a single "steady state" depth dependent profile of mantle viscosity. Neither transient rheology nor, it would appear, lateral viscosity variations are required in order to explain these disparate viscosity dependent observations. Of course, this statement should not be misconstrued to imply that lateral viscosity variations do not exist! Neither should it be miscontrued to imply that there do not exist other geophysical observations that may be very sensitive to this influence.

References

Carter, W. E., D. S. Robertson, T. E. Pyle, and J. Diamante, The application of geodetic radio interferometric surveying to the monitoring of sea-level, *Geophys. J. R. Astron. Soc.*, *87*, 3-13, 1986.

Cathles, L. M., *The Viscosity of the Earth's Mantle*, Princeton Univ. Press, Princeton, N. J., 1975.

Cheng, M. K., R.J. Eanes, C.K. Shum, B.E. Schutz, and B.D. Tapley, Temporal variations in low degree zonal harmonics from Starlette orbit analysis, *Geophys. Res. Lett.*, *16*, 393-396, 1989.

Corrieu, V., C. Thoraval, and Y. Ricard, Mantle dynamics and geoid Green functions, *Geophys. J. Int.*, *120*, 516-523, 1995.

Dickman, S. R., Secular trend of the Earth's rotation pole: Consideration of motion of the latitude observatories, *Geophys. J. R. Astron. Soc.*, *51*, 229-244, 1977.

Dziewonski, A. M., and D. L. Anderson, Preliminary reference Earth model, *Phys. Earth Planet. Inter.*, *25*, 297-356, 1981.

Forte, A. M., and W. R. Peltier, Plate tectonics and aspherical earth structure: The importance of poloidal-toroidal coupling, *J. Geophys. Res.*, *92*, 3645-3679, 1987.

Forte, A. M., and W. R. Peltier, Core-mantle boundary tomograph and whole mantle convection, *Geophys. Res. Lett.*, *16*, 621-624, 1989.

Forte, A. M., and W. R. Peltier, Viscous flow models of global geophysical observables, 1, Forward problems, *J. Geophys. Res.*, *96*, 20,131-20,159, 1991.

Forte, A. M., and W. R. Peltier, The kinematics and dynamics of poloidal-toroidal coupling in mantle flow: The importance of surface plates and lateral viscosity variations, *Adv. Geophys.*, *36*, 1-119, 1994.

Gegout, P., and A. Cazenave., Geodynamic parameters derived from 7 years of laser data on LAGEOS, *Geophys. Res. Lett.*, *18*, 1739--1742, 1991.

Goldstein, H., *Classical Mechanics*, Addison-Wesley, Reading, Mass., 1980.

Han, D., and J. Wahr, The viscoelastic relaxation of a realistically stratified earth, and a further analysis of postglacial rebound, *Geophys. J. Int.*, *120*, 287-311, 1995.

Haskell,, N. A., The motion of a viscous fluid under surface load, *Physics*, *6*, 265-269, 1935.

Imbrie, J., N. J. Shackleton, N. G. Pisias, J. J. Morley, W. L. Prell, D.G. Martinson, J. D. Hays, A. McIntyre, and A. C. Mix, The orbital theory of Pleistocene climate: Support from a revised chronology of the marine $\delta^{18}0$ record, in *Milankovicth and Climate*, edited by A. Berger et al., pp. 269-305, D. Reidel, Norwell, Mass., 1984.

Markowitz, W., Latitude and longitude, and the secular motion of the pole, *Methods Tech. Geophys.*, *1*, 325-361, 1960.

Meier, M. F., Contribution of small glaciers to global sea level, *Science*, *226*, 1418-1421, 1984.

Mikhailov, A. A., On the motion of the Earth's poles, *Astron. Zh.*, *48*, 1301-1304, 1971.

Mitrovica, J. X., and W. R. Peltier, On postglacial geoid subsidence over the equatorial oceans, *J. Geophys. Res.*, *96*, 20,053-20,071, 1991.

Mitrovica, J. X., and W. R. Peltier, Present-day secular variations in the zonal harmonics of the Earth's geopotential, *J. Geophys. Res.*, *98*, 4509-4526, 1993a.

Mitrovica, J. X., and W. R. Peltier, The inference of mantle viscosity from an inversion of the Fennoscandian spectrum, *Geophys. J. Int.*, *114*, 45-62, 1993b.

Mitrovica, J. X., and W. R. Peltier, Constraints on mantle viscosity based upon the inversion of post-glacial uplift data from the Hudson Bay region, *Geophys. J. Int.*, *122*, 353-377, 1995.

Morrison, L. V., Rotation of the Earth and the constancy of G, *Nature*, *241*, 519-520, 1973.

Muller, P. M., and F. R. Stephenson, The acceleration of the Earth and Moon from early observations, in *Growth Rhythms and History of the Earth's Rotation*, edited by G.D. Rosenburg and S. K. Runcorn, pp. 459-534, John Wiley, New York, 1975.

Munk, W. H. and G. F. MacDonald, *The Rotation of the Earth*, Cambridge Univ. Press, New York, 1960.

Newton, R. R., The Earth's acceleration as deduced from al-Biruni's solar data, *Mem. R. Astron. Soc.*, *76*, 99-128, 1972.

Nakiboglu, S. M., and K. Lambeck, Deglaciation effects on the rotation of the Earth, *Geophys. J. R. Astron. Soc.*, *62*, 49-58, 1980.

Pari, G., and W. R. Peltier, The heat flow constraint on mantle tomography based convection models: Toward a geodynamically self-consistent inference of mantle viscosity, *J. Geophys. Res.*, *100*, 12,731-12,751, 1995.

Peltier, W. R., The impluse response of a Maxwell Earth, *Rev. Geophys.*, *12*, 649-669, 1974.

Peltier, W. R., Glacial isostatic adjustment, 2, The inverse problem, *Geophys. J. R. Astron. Soc.*, *46*, 669-706, 1976.

Peltier, W. R., Dynamics of the ice age Earth, *Adv. Geophys.*, *24*, 1-146, 1982.

Peltier, W. R., Constraint on deep mantle viscosity from Lageos acceleration data, *Nature*, *304*, 434-436, 1983.

Peltier, W. R., The Lageos constraint on deep mantle viscosity: Results from a new normal mode method for the inversion of viscoelastic relaxation spectra, *J. Geophys. Res.*, *90*, 9411-9421, 1985.

Peltier, W.R., Global sea level and Earth rotation, *Science*, *240*, 895-901, 1988.

Peltier, W. R., Mantle viscosity, in *Mantle Convection*, edited by W. R. Peltier, pp. 857, Gordon and Breach, New York, 1989.

Peltier, W. R., Ice age paleotopography, *Science*, *265*, 195-201, 1994.

Peltier, W. R., and X. Jiang, The precession constant of the Earth: Variations through the ice-age, *Geophys. Res. Lett.*, *21*, 2299-2302, 1994.

Peltier, W. R., W. E. Farrell and J. A. Clark, Glacial isostasy and relative sea level: A numerical calculation, *Tectonophysics*, *50*, 81-110, 1978.

Peltier, W. R., R. A. Drummond, and A. M. Tushingham, Post-Glacial rebound and transient lower mantle rheology, *Geophys. J. R. Astron. Soc.*, *87*, 79-116, 1986.

Peltier, W. R., G. Pari and A. M. Dziewonski, Seismic tomography and mixing in the deep Earth, *Nonlinear Processes Geophys.*, in press, 1995.

Proverbio, E., and V. Quesada, Secular variation in latitudes and longitudes and continental drift, *J. Geophys. Res.*, *79*, 4941-4943, 1974.

Ricard, Y., C. Vigny, and C. Froidevaux, Mantle heterogeneities, geoid, and plate motion: A Monte Carlo inversion, *J. Geophys. Res.*, *94*, 13,739-13,754, 1989.

Richards, M. A., and B. H. Hager, Geoid anomalies in a dynamic Earth, *J. Geophys. Res.*, *89*, 5987-6002, 1984.

Rubincam, D. R., Postglacial rebound observed by Lageos and the effective viscosity of the lower mantle, *J. Geophys. Res.*, *84*, 437-447, 1984.

Sabadini, R., and W. R. Peltier, Pleistocene deglaciation and the Earth's rotation: Implications for mantle viscosity, *Geophys. J. R. Astron. Soc.*, *66*, 53-578, 1981.

Shackleton, N. J., Oxygen isotope analyses and Pleistocene temperatures readdressed, *Nature*, *215*, 15-17, 1967.

Shackleton, N. J., A. Berger, and W. R. Peltier, An alternative astronomical calculation of the lower pleistocene timescale based on ODP site 677, *Trans. R. Soc. Edinburg Earth Sci.*, *81*, 251-261, 1990.

Spada, G., R. Sabadini, D. A. Yuen, and Y. Ricard, Effects on post-glacial rebound from the hard rheology in the transition zone, *Geophys. J. Int.*, *109*, 683-700, 1992.

Stephenson, F. R. and L. V. Morrison, Long-term fluctuation in the Earth's rotation: 700 BC to AD 1990, *Philos. Trans. R. Soc. London A*, *351*, 165-202, 1995.

Tarantola, A. and B. Valette, Inverse problems = quest for information, *J. Geophys.*, *50*, 159-170, 1982*a*.

Tarantola, A. and B. Valette, Generalized non-linear inverse problems solved using the least squares criterion, *Rev. Geophys. Space Phys.*, *20*, 219-232, 1982*b*.

Tushingham, A. M., and W. R. Peltier, ICE-3G: A new global model of late Pleistocene deglaciation based upon geophysical predictions of postglacial relative sea level change, *J. Geophys. Res.*, *96*, 4497-4523, 1991.

Vincente, R. O., and S. Yumi, Co-ordinates of the pole (1899-1968), returned to the conventional international origin,, *Publ. Int. Latitude Obs. Mizusawa*, *7*, 41-50, 1969.

Vondrak, J., Long-period behaviour of polar motion between 100.0 and 1984.0, *Ann. Geophys.*, *3*, 351-356, 1984.

Wu, P., and W. R. Peltier, Pleistocene deglaciation and the Earth's rotation: A new analysis, *Geophys. J. R. Astron. Soc.*, *76*, 753-792, 1984.

Yoder, C. F., J. G. Williams, J. O. Dickey, B. E. Schutz, R. J. Eanes, and B. D. Tapley, Secular variation of the Earth's gravitational harmonic J_2 coefficient from Lageos and non tidal acceleration of Earth rotation, *Nature*, *303*, 757-762, 1983.

Yuen, D. A., and R. C. A. Sabadini, Viscosity stratification of the lower mantle as inferred by the $\dot{J}_2$ observation, *Ann. Geophys.*, *3*, 647-654, 1985.

X. Jiang and W.R. Peltier, Department of Physics, University of Toronto, 60 St. George St., Toronto, Ontario, Canada M5S 1A7. (e-mail: peltier@atmosp.physics.utoronto.ca)

(Received November 28, 1994; revised May 30, 1995; accepted June 21, 1995.)

JOURNAL OF GEOPHYSICAL RESEARCH, VOL. 102, NO. B5, PAGES 10,101–10,103, MAY 10, 1997

Correction to "Glacial isostatic adjustment and Earth rotation: Refined constraints on the viscosity of the deepest mantle" by W. R. Peltier and Xianhua Jiang

W. R. Peltier

Department of Physics, University of Toronto, Toronto, Ontario, Canada

In the paper "Glacial isostatic adjustment and Earth rotation: Refined constraints on the viscosity of the deepest mantle" by W. R. Peltier and Xianhua Jiang (*Journal of Geophysical Research*, *101*(B2)3, 269–329, 1996), there were a number of flaws in the numerical results. Since these could be annoying to the reader, it is important that the corrections to be described herein be put on record. The problems that have been identified concern Figures 6, 7, 8, and 9 and involve the issue of the nature of the viscosity contrast across the mantle that is required to fit the observed nontidal acceleration of planetary rotation (or equivalently $\dot{J}_2$) and the observed speed of polar wander that is currently taking place toward Greenland at a rate near 0.95°/Myr. None of the new theory reported in the paper, which involved a complete analysis of the rotational response to the ice age cycle using models that are fully triaxial, requires modification in consequence of the required corrections.

Figure 6 of Peltier and Jiang is to be replaced by Figure 1 herein. This shows the perturbations of inertia I^R_{13}, I^R_{23}, and I^R_{33} that are derived on the basis of the SPECMAP $\delta^{18}O$ record when the last deglaciation event (which began 21 kyr before present) is constrained by the ICE-4G model of *Peltier* [1994, 1996]. These time series are denoted by the solid lines, and they are compared on Figure 1 to the results for a simple periodic sawtooth model (dashed lines) of the same kind that has previously been invoked [e.g., *Wu and Peltier*, 1984; *Peltier*, 1988] in earlier analyses of the same observational data. Comparing this new Figure 1 with the original Figure 6 of Peltier and Jiang, the reader will note an error in the labeling of the ordinate in Figure 6b. The results for the sawtooth model, now shown explicitly on Figure 1 herein, replace the LGM values shown on Table 1 of Peltier and Jiang.

Figures 2a and 2b herein show the results that replace those shown previously in Figures 7c and 8b of Peltier and Jiang. In these analyses, simple two-layer models for mantle viscosity have been employed in which the viscosity in the layer from the base of the lithosphere to 670 km depth is assumed to be equal to 1×10^{21} Pa s, and the theory is used to predict $\dot{J}_2$ as a function of the assumed constant value of the viscosity in the lower mantle beneath the depth of 670 km. A focus of the analysis of Peltier and Jiang was on the impact upon the inferred value of lower mantle viscosity of treating the ocean loading component of the rotational excitation in a gravitationally self-consistent way. This variation of the analysis procedure, as suggested by Peltier and Jiang, has no significant impact upon the results for $\dot{J}_2$. These results, shown in Figure 1a for both the SPECMAP (solid line) and sawtooth (dashed line) based representations of the forcing, demonstrate that a good fit to the observations is obtained for lower mantle viscosities near 2×10^{21} Pa s and near 10^{23} Pa s. The shift in the values for lower mantle viscosity obtained when the sawtooth load replaces the SPECMAP load is small. There is no essential difference in these results from those reported by Peltier and Jiang.

Figure 2b herein shows the results that replace those shown on Figure 7c of Peltier and Jiang. These results are for polar wander speed as a function of lower mantle viscosity, and again results are shown for both the SPECMAP based model of the forcing (solid line) and for the sawtooth model of the forcing (dashed line). Once more the main result of Peltier and Jiang is confirmed by the reanalyses reported herein, namely, that the polar wander data are fit by the same lower-viscosity contrast as was shown to fit the $\dot{J}_2$ observation. The higher contrast solution for $\dot{J}_2$ is ruled out by the polar wander observation. An important difference does exist between the results shown in Figure 2b herein, however, and that presented by Peltier and Jiang. This concerns the shape of the curve of present-day polar wander speed as a function of lower mantle viscosity. For the new results shown on Figure 2b this curve does not fall rapidly to zero as the viscosity of the lower mantle is increased above the value which is required to fit the observations. Rather it develops a plateau such that the present-day predicted polar wander speed does not decrease substantially until lower mantle viscosity is significantly increased. This shape for the polar wander speed versus lower mantle viscosity curve is now essentially identical to the dependence obtained by *Peltier* [1988], whose earliest analysis of this issue was based upon the use of disc load approximations to the histories of the continental ice sheets involved in the glaciation-deglaciation cycle. It is also important to note two further pieces of information presented on Figure 2b, namely, that the use of the sawtooth approximation to the loading history (dashed line) shifts the plateau upward such that a wide range of values of lower mantle viscosity now fits the observation and that the incorporation of fully self-consistent ocean loading into the computation of the perturbations of inertia similarly shifts the plateau to lower values of velocity (curve denoted by asterisks). That the same plateau structure exists in the polar wander speed versus lower mantle viscosity curve for accurate models of the deglaciation history as previously obtained by *Peltier* [1988] for simple models could prove extremely important in reconciling observed rotation effects to modern observations of secular sea level rise.

Figures 2c and 2d herein present the results that replace those shown in Figure 9 of Peltier and Jiang. These are analogous in every way to those shown on Figures 1a and 1b, respectively, and differ from them only in that the boundary between the two viscous layers of the mantle is taken to be located at 1400 km depth rather than at 670 km depth. Once more these results show that the viscosity contrasts required by

Paper number 97JB00620.
0148-0227/97/97JB-00620$09.00

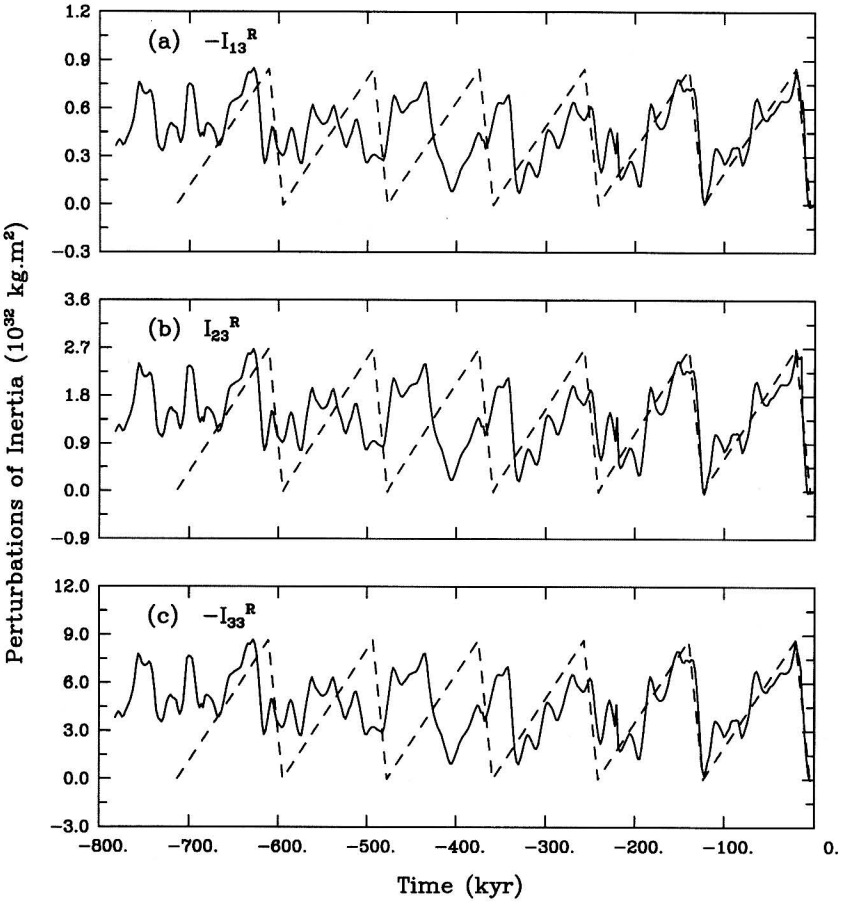

Figure 1. Time series of perturbations of inertia based upon two different models of the glaciation-deglaciation process, one based upon the SPECMAP $\delta^{18}O$ record (solid lines) and a second based upon a simple sawtooth approximation to the SPECMAP record (dashed lines). In each case the portion of the record from last glacial maximum until the present is constrained to match the ICE-4G model of *Peltier* [1994, 1996]. This replaces Figure 6 of Peltier and Jiang.

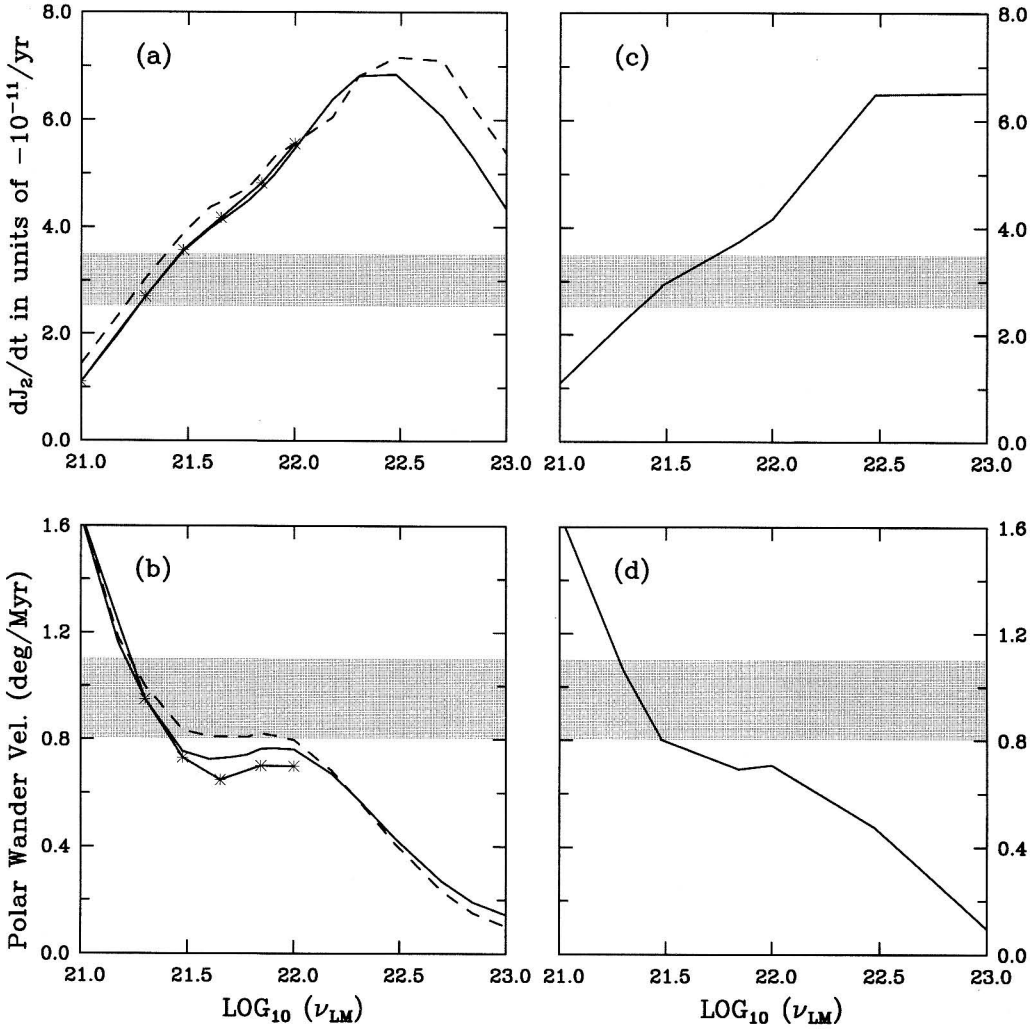

Figure 2. (a) Present-day $\dot{J}_2$ as a function of lower mantle viscosity for a suite of models which have upper mantle and transition viscosity fixed to the value 1×10^{21} Pa s. The results shown as the solid line have been obtained with the deglaciation history constrained to SPECMAP (see Figure 1), whereas those shown as the dashed line are based upon the sawtooth approximation to the history. The line on which the individual points are denoted by asterisks is the result obtained using ocean loading histories that are fully consistent with the mantle viscosity profile; otherwise, all results shown employ the same ocean loading contribution to the total forcing as was obtained in the gravitationally self-consistent calculation in which the lower mantle viscosity was fixed to the value 2×10^{21} Pa s. The observed $\dot{J}_2$ is shown as the hatched region. (b) Present-day polar wander speed as a function of the viscosity beneath 670 km depth for the same sequence of models as employed in Figure 2a. (c) Same as Figure 2a but with the interface in viscosity at 1400 km depth rather than at 670 km depth. The viscosity above 1400 km depth has been fixed to the value 1×10^{21} Pa s. (d) Same as Figure 2b but with the interface in viscosity at 1400 km depth. This replaces Figures 7, 8, and 9 of Peltier and Jiang.

the $\dot{J}_2$ and polar wander speed observations are fully compatible. However, the increase in contrast required when the viscosity in the upper layer is fixed to 10^{21} Pa s is considerably lower than that shown on Figure 9 of Peltier and Jiang. That such a small increase in contrast should have been expected is in fact clear on the basis of the Fréchet derivatives for $\dot{J}_2$ and polar wander speed shown in Figure 10 of Peltier and Jiang. The result in Figure 9 of Peltier and Jiang is in fact incompatible with the results in Figure 10b which shows viscosity profiles obtained on the basis of formal inversions of multiple data sets pertaining to the postglacial rebound phenomenon. These results, discussed more fully by *Peltier and Jiang* [1996] and *Peltier* [1996], are entirely unaffected by the corrections to Peltier and Jiang reported herein.

References

Peltier, W. R., Global sea level and earth rotation, *Science*, *240*, 895–901, 1988.

Peltier, W. R., Ice-age paleotopography, *Science*, *265*, 195–201, 1994.

Peltier, W. R., Mantle viscosity and ice-age ice sheet topography, *Science*, *273*, 1359–1364, 1996.

Peltier, W. R., and X. Jiang, Mantle viscosity from the simultaneous inversion of multiple data sets pertaining to postglacial rebound, *Geophys. Res. Lett.*, *23*, 503–506, 1996.

Wu, P., and W. R. Peltier, Pleistocene deglaciation and the Earth's rotation: A new analysis, *Geophys. J. R. Astron. Soc.*, *76*, 202–242, 1984.

(Received February 19, 1997.)